Title:

Experience replay facilitates the rapid formation of multi-scale hexagonal patterns of grid cells

Short title:

Experience replay facilitates the formation of hexagonal patterns

Authors & Affiliations:

Bo Zhang[1,2,3], Lei Ma[1,4], and Jia Liu[2*]

[1] Beijing Academy of Artificial Intelligence, Beijing, 100084, China

[2] Tsinghua Laboratory of Brain and Intelligence & Department of Psychology, Tsinghua University, Beijing, 100084, China

[3] Division of Humanities and Social Sciences, California Institute of Technology, Pasadena, CA 91125

[4] National Biomedical Imaging Center, College of Future Technology, Peking University, Beijing, 100871, China

Contact Information:

*Correspondence shall be addressed to: JL, liujiathu@tsinghua.edu.cn

Keywords:

Reverse replay, Grid cell, Hippocampus, Entorhinal Cortex, Neural circuits, Continuous attractor model

Abstract

Experience replay, characterized by the sequential reactivation of hippocampal place cells, has been proposed to consolidate past experiences and simulate future scenarios, thereby constructing cognitive maps to guide action. However, the role of experience replay in the formation of hexagonal patterns of entorhinal grid cells – known to serve as the metrics of cognitive map – remains largely unknown. Here, we used continuous attractor models to simulate the formation of multi-scale hexagonal patterns, and investigated the regularity of generated patterns by directly modulating experience replay of hippocampal place cells in awake state. We found that reverse replay significantly increased the regularity of small-scale hexagonal patterns compared to conditions with no replay, forward replay, and shuffled replay of past experiences. In contrast, large-scale hexagonal patterns emerged spontaneously, independent of experience replay. Further analysis revealed that the efficiency of reverse replay in hexagonal pattern formation was influenced by the interaction between grid scales and the amount of past experience. Specifically, reverse replay maintained excitatory and inhibitory grid cell activity during pattern translation when the amount of past experience was limited, making it particularly efficient for the rapid formation of small-scale hexagonal patterns. In summary, our results suggest a potential link between experience replay and the formation of multi-scale hexagonal patterns from a computational perspective. These findings may provide insights into the role of grid cell signals in visual attention and the rapid adaptation of hexagonal patterns in scene transition.

Introduction

Episodic memory, closely associated with the hippocampus (HPC; Tulving and Markowitsch, 1998; Burgess et al., 2002), is metaphorically described as mental travel on a cognitive map (Tolman, 1948; Moser et al., 2017). This cognitive ability depends on the place cell replay in the hippocampus, which organizes experiences into relational structures for retrieving the past and imagining the future (Fig.1a; Foster and Wilson, 2006; Diba and Buzsáki, 2007; Schacter et al., 2007; Carr et al., 2011; Mattar and Daw, 2018; Pfeiffer, 2020). The sequential representations of the hippocampal replay have been associated with the topological structure of novel environment (Wu and Foster, 2014), the factorized representation of objects (Liu et al., 2019), the re-organization of non-local experiences into planning (Liu et al., 2021), and compositional computation (Kurth-Nelson et al., 2023). Impaired hippocampal replay leads to deficits in sequential representations, as observed in both schizophrenia patients (Nour et al., 2021) and rodent models (Suh et al., 2013). However, the mechanism of hippocampal replay in constructing a cognitive map has been less discussed.

The relational structures of experience, fundamental to the cognitive map (Hafting et al., 2005; McNaughton et al., 2006; Behrens et al., 2018), are associated with the entorhinal grid cells to map the external environment with hexagonal metrics (Fig.1c; Bellmund et al., 2019; Bellmund et al., 2020; Peer et al., 2021; Whittington et al., 2022), where experiences are represented by the multi-hexagonal scales underlying positional encoding (Fiete et al., 2008; Bush et al., 2015; Stemmler et al., 2015; Bicanski and Burgess, 2019). These hexagonal structures have shown strong associations with place cell activity. In the spatial domain, the hexagonal regularity and spatial scale of grid cells decreased as a function of environmental novelty (Barry et al., 2012), which has been known to track the firing rate of CA1 place cells (Larkin et al., 2014). In the time domain, grid cell activity was elicited by visual attention within a time range of milliseconds to seconds (Nau et al., 2018; Killian & Buffalo, 2018; Staudigl et al., 2018; Julian et al., 2018; Wilming et al., 2018), implicating the capacity of grid cell in rapid forming the hexagonal patterns. Meanwhile, the hippocampal replays of place cell were observed within the same time range, either during movements on a linear-track (Pfeiffer, 2020) or following the first lap of a U-shaped track (Foster & Wilson 2006) in goal-directed navigation. Particularly, early postnatal development suggests that grid cells emerge abruptly in the awake state around day P20, followed by the reliable emergence of sequential replay between P19 and P20 (Farooq & Dragoi, 2019). In mature brains,

grid cells and place cells were coordinated during hippocampal replay. Grid cell activity was spatially coherent with place cell activity, with an average of 11ms delay, suggesting a propagation of replay sequence from the hippocampus to the entorhinal cortex in awake state (Ólafsdóttir et al., 2016). These empirical findings may reflect a major involvement of hippocampal replay in forming the hexagonal regularity and the multi-scale organization of grid cell.

To test this conjecture, we simulated the formation of multi-scale hexagonal pattern of grid cell using continuous attractor networks (CAN) (Burak and Fiete, 2009; Couey et al., 2013; Kang and Balasubramanian, 2019; Khona et al., 2021), which is commonly referred to as the classic spin-glass model (Fuhs and Touretzky, 2006). Meanwhile, hippocampal replay was simulated by sequential place cell activity that represents past visited spatial locations. A place cell at each location was modelled to connect with a grid cell from one of four spatial scales (Fig.1c, scale [i.e., Mod] I, II, III, and IV; Fiete et al., 2008; Stemmler et al., 2015; Bush et al., 2015). The excitatory and inhibitory synaptic plasticity of grid cells was independently updated within each spatial scale. With the endeavor proving challenging in empirical studies, we examined the regularity of the generated hexagonal pattern, indexed by grid score, under four types of replay conditions (i.e., No-, Forward-, Reverse-, and shuffled-replay) and two types of experiences (i.e., limited or extended exploration defined either by the number of locations or directions). Limited exploration was intentionally used to investigate the rapid formation of hexagonal patterns in eye movements (Nau et al., 2018; Killian & Buffalo, 2018; Staudigl et al., 2018; Julian et al., 2018; Wilming et al., 2018) and one-dimensional linear tracks (Yoon et al., 2016; Jacob et al., 2019) as compared to full exploration of the environment (i.e., extended exploration; Hafting et al., 2005; Kang and Balasubramanian, 2019). The present design allows investigations of the potential link between experience replay and the formation of hexagonal patterns of grid cell by intentionally activating or deactivating place cell activity.

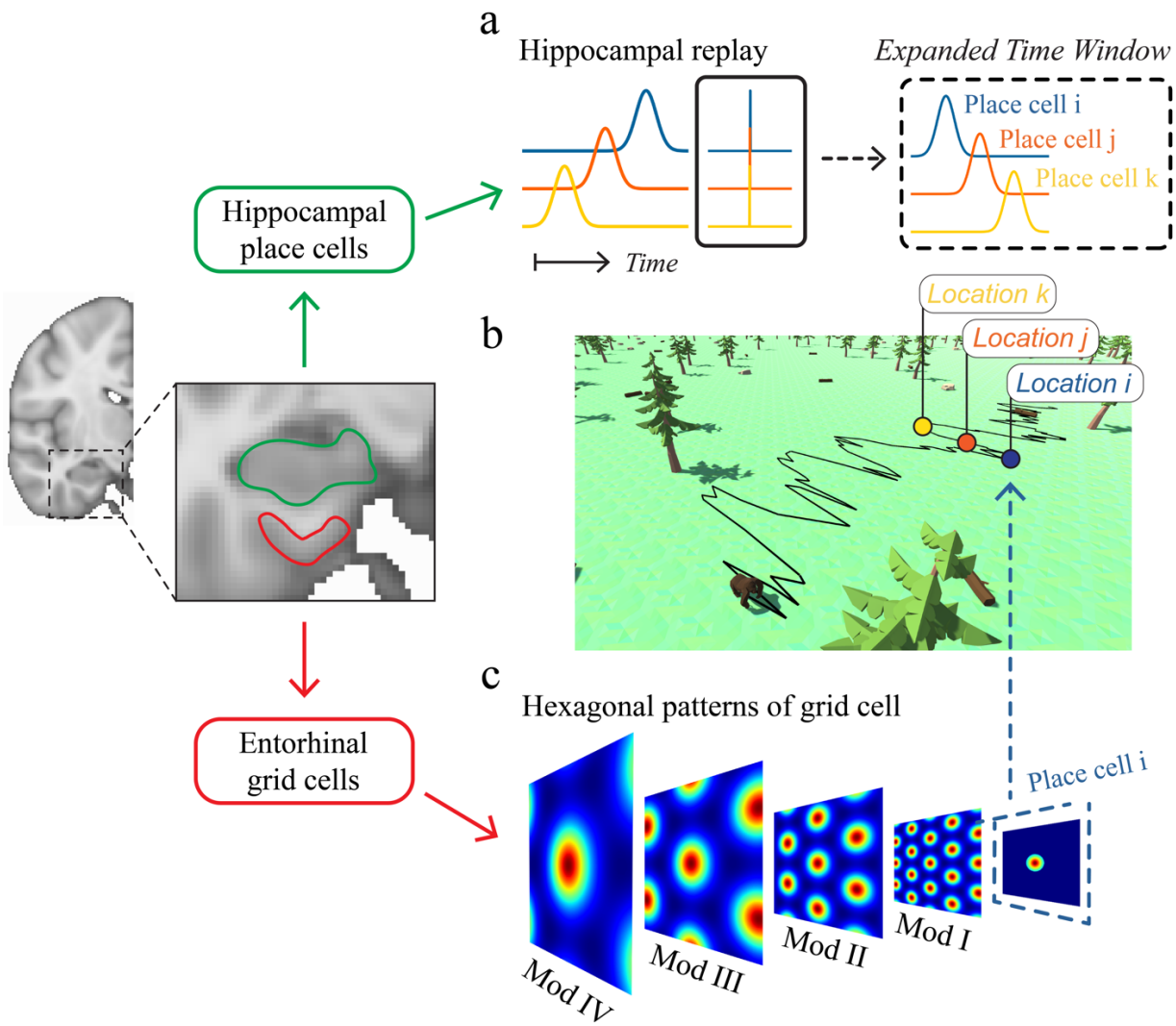

Figure 1. Place cell replay in the hippocampus and multi-scale hexagonal patterns of grid cells in the entorhinal cortex. (a) Schematic of reverse experience replay of place cells k, j, i (Foster and Wilson, 2006; Diba and Buzsáki, 2007; Schacter et al., 2007; Carr et al., 2011). These place cell activities, denoted by colored lines, are replayed in a reversed temporal order (i-j-k) relative to original experiences (k-j-i) at the pause location (blue point shown in b). (b) Schematic of a virtual space, where predefined movement trajectory is projected into a squared open space for pattern translation of hexagonal patterns. (c) Schematic of multi-scale hexagonal patterns of grid cells. These grid cells, which connect to a place cell encoding location i (Solstad et al., 2006; Rolls et al., 2006; Bush et al., 2015; blue point shown in d), are activated when the agent visits location i.

Results

We first examined the effect of No-replay, Forward-replay, and Reverse-replay on the formation of hexagonal patterns under limited exploration. The model received a sequence of place cell activations as inputs, simulating "walking" experiences during pattern translation in randomized allocentric directions (i.e., 70°, 115°, or 160° with 0° pointing East) (Fig.2a). Each "walking" experience consisted of either 5, 10, or 15 location movements, resulting in an average of 10 location movements in each direction and a total of 1200 movements in each simulation. The final visit of each experience was designated as the pause locations to mimic the animal's decision point. In the No-replay condition, only the actual "walking" experiences were applied to the model. In contrast, the Forward-replay and Reverse-replay conditions examined the direction-dependency of replay. In these two conditions, the model received an additional "walking" experience identical to the actual one, preceding the movements in the forward direction and following the movements in the reverse direction, respectively (Foster & Wilson, 2006; Ambrose et al., 2016; Gillespie et al., 2021). The spatial regularity of the hexagonal patterns generated in each condition was assessed through 15 independent simulations.

The result revealed that the Reverse-replay condition promoted the formation of hexagonal patterns across all grid scales. The grid scores showed a rapid increase at the beginning of simulations and remained significant over 1200 movements (Fig.2b & c & Fig.S2a, mean grid score of Mod I / Mod II / Mod III / IV = 1.39 / 1.44 / 1.43 / 1.39, respectively; $p<0.05$, initial threshold, $p < 0.05$; corrected for multiple comparisons). Next, we further accessed the group-level regularity of hexagonal patterns using the toroidal topology detection procedure (Gardner et al., 2022). The joint activity of rats' grid cells was found to reside on a toroidal manifold, consistent with prediction of the twisted torus model (Samsonovich and McNaughton, 1997; McNaughton et al., 2006; Knierim and Zhang, 2012; Khona & Fiete, 2022; Gardner et al., 2022; Sorscher et al., 2023). Specifically, we observed a significant toroidal structure based on the dimensionality-reduced population activity of CAN-generated grid cells in each spatial scale (Fig.2d, Fig.S3, see Method for details). This was indicated by the significant lifespans of barcodes (highlighted with red bars) for one 0D hole (H^0, the entire torus as a connected object), two 1D holes (i.e., H^1, the two blue lines warped around the circular axis and representing the inner and outer hole of the torus) and one 2D hole (H^2, the entire surface of the torus enclosed by two 1D holes that forms the cavity within the torus) compared to the threshold derived from shuffled activity distribution,

corrected for multiple comparisons. These findings confirmed the successful formation of multi-scale hexagonal patterns of grid cell population in the Reverse-replay condition, even with constrained environmental exploration.

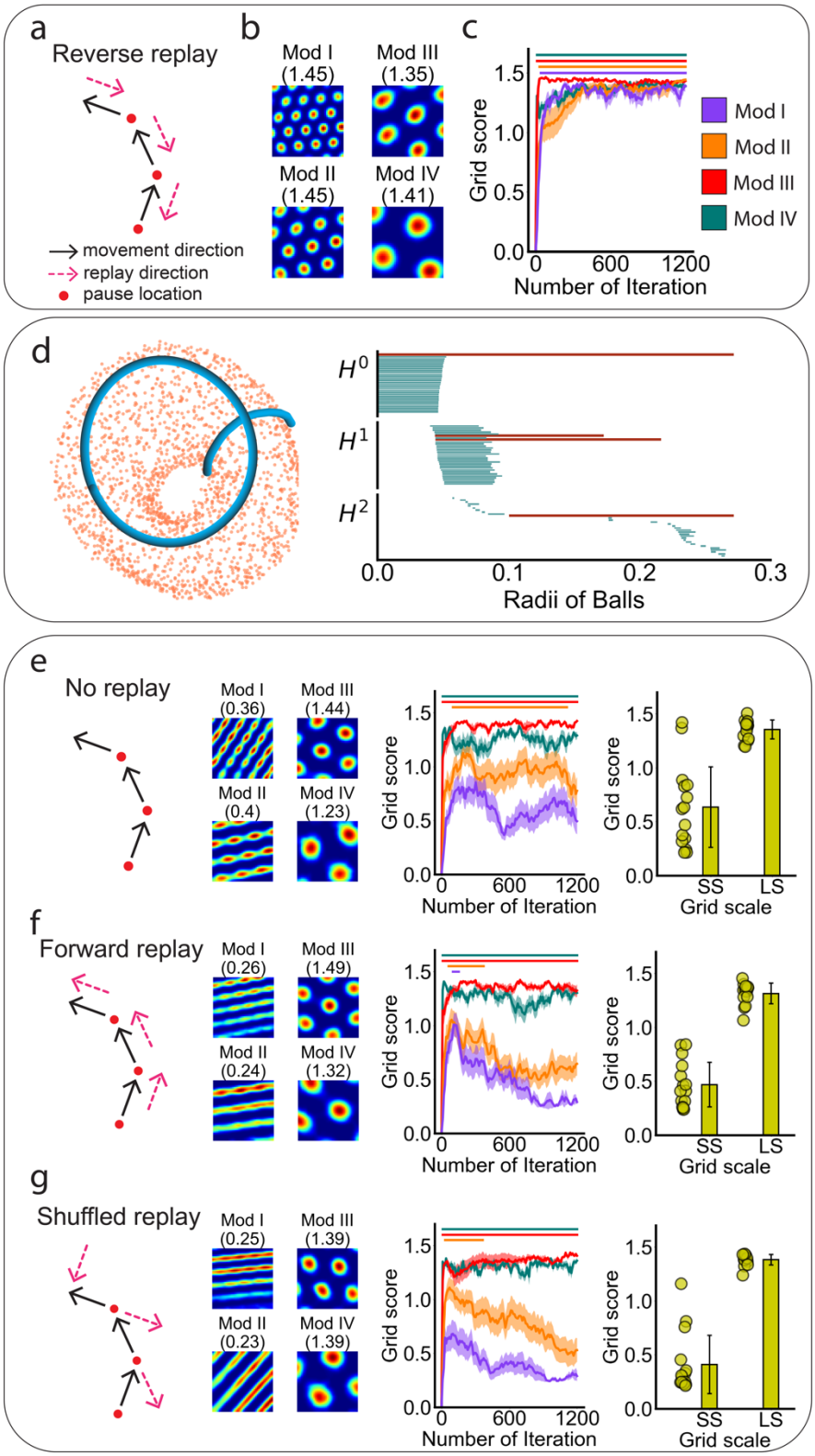

Figure 2. Impact of experience replay on multi-scale hexagonal pattern formation with a limited exploration. (a) Schematic of movement trajectories. Black arrows denote the movement direction,

and red arrows denote the replay direction. (b) The multi-scale hexagonal patterns generated with reverse replay. Values in brackets indicate grid scores. (c) The grid scores, averaged across grid scales and simulations, increased as a function of the number of model iterations. Solid lines at the top indicate significant grid scores ($p < 0.05$, initial threshold, $p < 0.05$; corrected for multiple comparisons). Error bars denote standard error. (d) Example of a toroidal structure derived using dimensionality reduction based on population activity of CAN-generated grid cells in Mod I. Barcodes, showing the top 30 holes with the longest lifespans from persistent cohomology, revealed one 0D hole (H^0), two 1D hole (H^1) and one 2D hole (H^2) with significantly long lifespans compared to the significant threshold (red bars), corrected for multiple comparisons. (e)-(g) Examples of the multi-scale hexagonal patterns of grid cell generated by CAN with either no replay (e), forward replay (f), or shuffled-experience replay (g), respectively. The bar charts show the averaged grid score. The dots denote the averaged grid score within one simulation. Note that all models underwent same number of iterations. SS (Mod I & II) and LS (Mod III and IV) denotes small- and large-scale, respectively.

In contrast, the No-replay and Forward-replay conditions resulted in deficits in hexagonal pattern formation particularly at small scales (i.e., grid Mod I & II; No-replay: Fig.2e & Fig.S2a, left panel, mean grid score of Mod I / Mod II = 0.49 / 0.77; Forward-replay: Fig.2f & Fig.S2a, left panel, mean grid score of Mod I / Mod II = 0.29 / 0.64). For both conditions, the grid scores of small-scale hexagonal patterns fluctuated during pattern translation after a transient increase at the beginning of simulations and eventually decreased, yielding a stripe pattern (Yang et al., 2004). By comparison, these two conditions generated regular hexagonal patterns at large scales (Mod III & IV), where grid scores were significantly higher than the shuffled threshold (No-replay: Fig.2e & Fig.S2a, right panel; mean grid score of Mod I / Mod II = 1.42 / 1.29; Forward-replay: Fig.2f & Fig.S2a, right panel, mean grid score of Mod III & IV = 1.32 / 1.30; $p<0.05$, initial threshold, $p < 0.05$; corrected for multiple comparisons).

To further investigate the impact of spatial-temporal structure of past experiences, we tested a Shuffled-experience condition in response to reverse replay. In this condition, replay directions were randomly drawn from past experiences within the simulation and were not necessarily reversed relative to the immediate past "walking" experience. The Shuffled-replay condition produced results similar to the No-replay and Forward-replay conditions. Stripe patterns were observed at small scales (i.e., grid Mod I & Mod II; Fig.2g & Fig.S2a, left panel, mean grid score of Mod I / Mod II = 0.29 / 0.53), whereas significant regularity of hexagonal patterns was observed at large scales (i.e., grid Mod III & Mode IV; Fig.2g & Fig.S2a, right panel, mean grid score of Mod III / Mod IV = 1.40 / 1.36; $p < 0.05$, initial threshold, $p < 0.05$; corrected for multiple comparisons).

Taken together, the No-replay, Forward-replay, and Shuffled-replay conditions produced significantly higher grid scores for large scale hexagonal patterns compared to that of small scales (Mod I & II versus Mod III & IV: $t(14) = 7.02 / 13.89 / 13.28$ for No-replay, Forward-replay, and Shuffled-replay, respectively, $p < 0.001$, two-sided), and the hexagonal patterns emerged from stripe patterns at small scales in the Reverse-replay condition. These findings suggest that the formation of multi-scale hexagonal patterns selectively favors Reverse-replay, characterized by a sequential replay opposite to actual experience. This presumably reflect the necessity of reverse experience replay in constructing a high-resolution cognitive map.

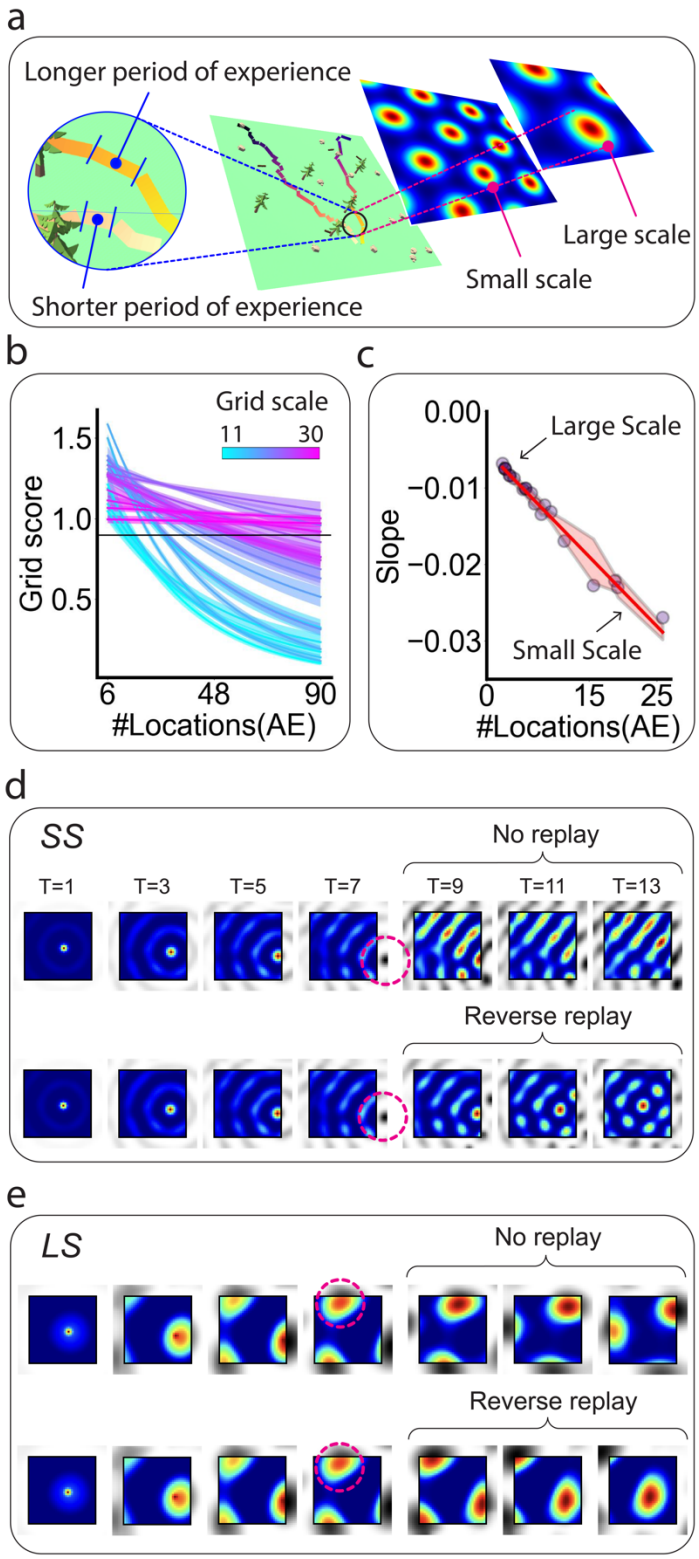

Figure 3. Impact of reverse replay on multi-scale hexagonal pattern formation with an extended number of visited locations. (a) Schematic of amount of experience (blue) and grid scale (purple).

(b) grid scores, changed as a function of experience-length and grid scale in the Reverse-replay condition, are fitted by an exponential decay function (R^2=0.62, P<.0.001). (c) The interaction of the number of movements and grid scale, indexed by the slope (i.e., decay rate), predicted the temporal dynamics of hexagonal pattern formation during iterations (R^2=98.66%, P<0.001). Error bar denotes standard error. (d) & (e) Schematic that illustrates how reverse replay influences the regularity of hexagonal patterns. In the small-scale (SS) condition (d). A receptive field (pink circle), formed during T1-5, was disrupted at T7 due to exceeding the boundary of representational space, and leading to a loss of information. Reverse replay maintained the excitatory and inhibitory dynamics of the receptive field during T9-13 by transferring current location representation to the neurons that represents visited locations. In the large scale (LS) condition (e), a receptive field (pink circle) was rapidly formed during T3-5 and propagated out of representational space at T7. The newly-formed receptive field emerged at T7, replacing the disrupted one and maintaining the excitation-inhibition dynamics of pattern formation, prevented the disruption of hexagonal pattern despite the disruption of earlier-formed receptive field.

Next, we examined the impact of reverse replay on the regularity of hexagonal patterns by linearly modulating the amount of experience (AE) and grid scales (GS). Specifically, we explored how grid scores varied as a function of the AE, indexed by the number of visited locations in each direction (Fig.3a, Left), and the GS, indexed by the size of grid cell receptive fields (Fig.3a, Right), under both No-replay and Reverse-replay condition. To achieve this, we conducted 1,160 CAN simulations on grid scores, systematically varying the modulator AE, GS, and the type of experience replay across 29 levels (6-90 locations [i.e., pixels]), 20 levels (11-30 pixels), and 2 conditions (No- & Reverse-replay), respectively (see Methods for details).

As expected, the results revealed significant main effects of replay ($F(1, 1152) = 147.5$, $P < 0.001$) and GS ($F(1, 1152) = 1376.2$, $P < 0.001$), both positively correlated with grid scores (Fig.S6), consistent with findings observed during limited exploration. Interestingly, a significant main effect of AE was also identified (Fig.S6; $F(1, 1152) = 324.8$, $P < 0.001$), with grid scores negatively correlated with AE in the Reverse-replay condition ($t(576) = -16.503$, $P < 0.001$), and maintaining constant in the No-replay condition ($t(576) = -1.910$, $P = 0.057$). These results highlighted the conditional efficiency of reverse replay in hexagonal pattern formation, dependent on AE, as indicated by a significant interaction ($F(1, 1152) = 155.9$, $P < 0.001$). To further assess AE's influence in the Reverse-replay condition, we calculated the decay rate of grid scores along AE, indexed by the slope *k*, and identified the smallest AE for each grid scale at which grid scores reached the significance threshold from the initial state (Fig.S7). The analysis revealed a significantly positive correlation between the decay slope *k* and grid scales ($R^2 = 0.62$, $P < 0.001$), indicating that smaller scale hexagonal patterns were associated with faster grid score decay (Fig.3b). Additionally, the decay slope *k* accurately predicted the AE preceding the experiences replay required to form regular hexagonal patterns (Fig.3c; R2=98.66%, P<0.001), demonstrating that large scale hexagonal pattern formed with small AEs, while small scale patterns required larger AEs. The maximum AE that enables the formation of small scale hexagonal pattern was approximately 25 locations, corresponding to an AE size ranging between half the space's edge and half its diagonal. This reflected the edge effect in hexagonal pattern formation (McNaughton et al., 2006; Foster and Wilson, 2006; Sorscher et al., 2019; Hägglund et al., 2019; Sorscher et al., 2023). In contrast, large scale hexagonal patterns formed rapidly with smaller AEs and were unaffected by edge effects (Fig.3c).

The above findings confirm the positive impact of reverse replay on the regularity of small scale hexagonal patterns across varying amount of past experiences (i.e., number of locations in a given direction). Furthermore, these results suggest a potential biological mechanism for the rapid tessellation of high resolution cognitive maps, resembling memory consolidation (Carr et al., 2011). Specifically, the reversed sequential activity of place cells appears to mitigate edge effect by activating connected grid cells, maintaining the excitatory and inhibitory dynamics of new-formed receptive fields. Through this mechanism, an infinitely large space can be folded into a periodic structure and represented by a limited number of neurons. For example, in the absence of reverse replay (Fig.3d, top row), the newly-formed receptive field at T5 lost its excitatory and inhibitory dynamics during pattern translation at T7, as exceeding the boundary of representational space. This disruption led to the disintegration of the developing hexagonal pattern into a stripe-like pattern (Fig.3d, top row; T9-T13). In contrast, reverse replay of past experiences preserved the receptive field by transferring location representations to neurons encoding previously visited locations (Fig.3d, bottom row; T9-T13). This process facilitated the continued development of the hexagonal pattern. On the other hand, large scale receptive fields were rapidly formed between T3 and T5 (Fig.3d, top row). At T7, a newly formed receptive field replaced the earlier ones that had propagated out of the representational space during pattern translation. This substitution prevented hexagonal pattern disruption even in the absence of reverse replay (Fig.3e, top row). In summary, our simulations demonstrate that reverse replay plays a critical role in balancing spatial (i.e., grid scale) and temporal (amount of past experience) demands for hexagonal pattern generation.

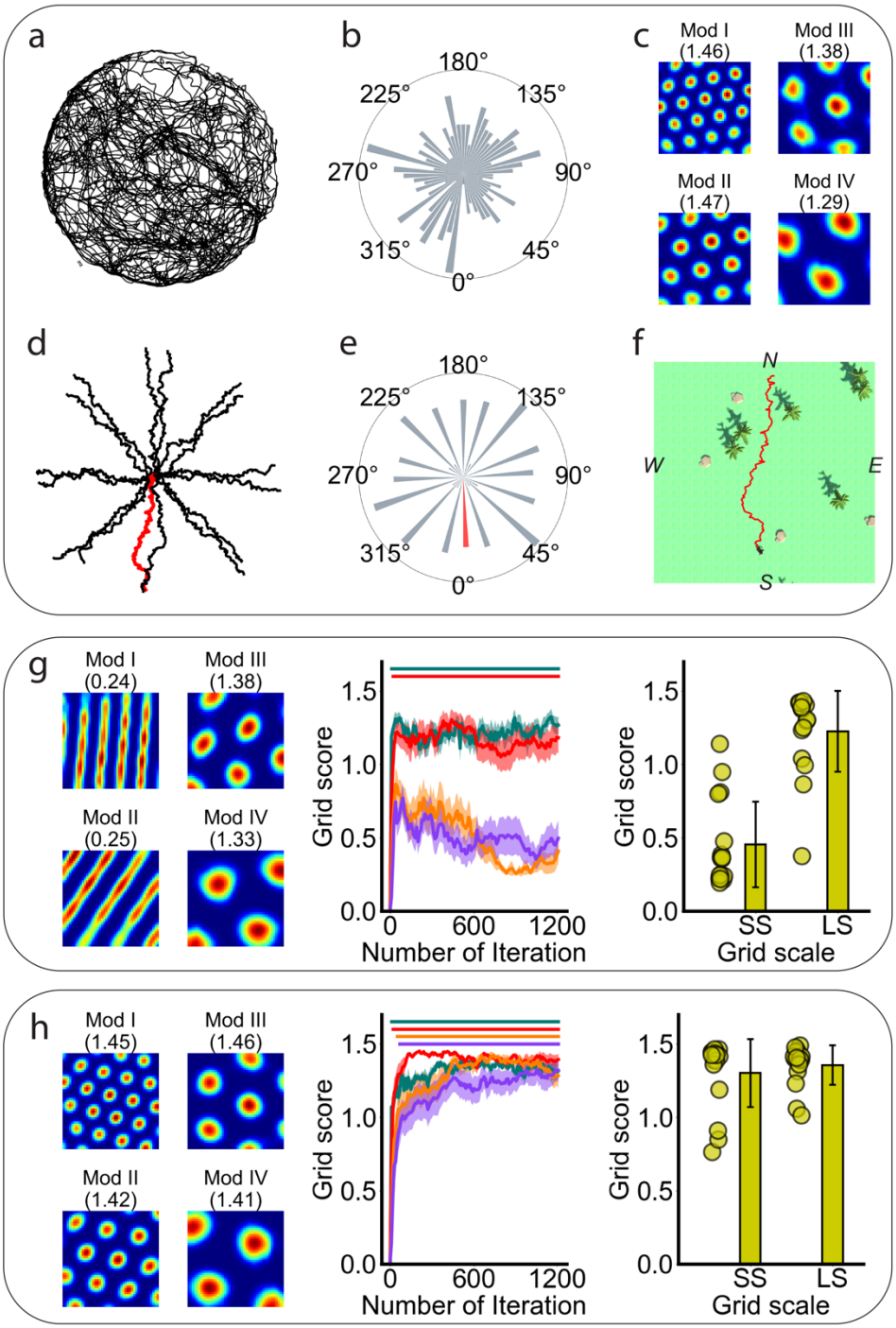

Figure 4. Impact of experience replay on multi-scale hexagonal pattern formation with an extended number of movement directions. (a) Rat trajectories, collected from the open-source dataset (Hafting et al., 2005), were used for CAN simulation. (b) Density distribution of rat's movement directions during the collection of scattered randomly thrown pieces of food ($p = 0.23$, Rayleigh test). (c) Multi-scale hexagonal patterns emerged in the absence of reverse replay; Grid scores are

shown in bracket. (d) Eight global directions, each associated with a series of "walking" experience dominated by the global direction and additional random noise between -90° and 90°. For instance, a global direction pointing South (highlighted in red) corresponded to homogeneous directions of 270° ± 90°. (e) Density distribution of movement directions used for CAN simulation. (f) An example of a trajectory with homogeneous movement directions (highlighted in red; $p < 0.001$, Rayleigh test). (g)-(h) Multi-scale hexagonal patterns generated by CAN in the No-replay condition (g) and the Reverse-replay condition (h), respectively. Line and bar charts show the averaged grid scores of four grid scales across 16 independent simulations (d-e). Note that same number of iterations was applied to all simulations.

To further validate the mechanism of reverse replay in representational transferring among neurons during pattern formation, we simulated the formation of hexagonal patterns under conditions of extended movement directions and the absence of reverse replay. The rationale for this analysis was based on the hypothesis implicated by the above results that high-frequency and diverse directional switching is more likely to maintain newly formed receptive fields within the representational space, thereby avoiding edge effect, compared to scenarios with homogeneous movement directions. If this hypothesis holds true, regular small scale hexagonal patterns should be generated despite the absence of reverse replay. Therefore, this analysis was conducted using an open-source dataset contributed by Hafting et al (2005) (Fig.4a), which contains a large number of animal's trajectories with diverse movement directions uniformly distributed across 0° to 360° (Fig.4b; $p = 0.23$, Rayleigh test). The trajectories were down-sampled to 1200 movement locations and scaled into the 45-by-45-pixel representational space to match the procedure used in earlier simulations. As expected, we observed a significant regularity in hexagonal patterns across all grid scales, even in the absence of reverse replay (Fig.4c, grid score= 1.46/1.47/1.38/1.29 for Mod I / II / III / IV, respectively. $p < 0.05$, initial threshold, $p < 0.05$; corrected for multiple comparisons). Notably, this result does not imply the absence of reverse replay when rats collect scattered randomly thrown pieces of food (Hafting et al., 2005). Instead, it highlights the potential neural mechanism underlying hexagonal pattern formation, suggesting that grid cells use representational transfer to maintain the excitatory and inhibitory dynamics of receptive fields.

Saturated exploration is not required in many scenarios. Therefore, we conducted a final simulations of hexagonal pattern formation by converging the range of movement directions into homogeneity. We predicted that stripe-like patterns would emerge in the absence of reverse replay at small scales, while the presence of reverse replay would restore the regularity of hexagonal patterns. To test this, we defined eight global directions that cover 360° with 45° intervals (Fig.4d, e). Each global direction condition was repeated twice (Fig.S8), and were paired with a series of intermediate "walking" experiences that included random noises between -90° and +90° (Fig.4f). This approach maintained the diversity in movement directions while excluding the possibility of representational transfer. As expected, the result revealed stripe-like patterns for small scales in the No-replay condition (Fig.4g, mean grid score of Mod I / Mod II = 0.49 / 0.41, respectively), leading to a significantly lower grid score than those of large scales (Fig.S2b; $t(15) = 7.47$, $p<0.001$, two-sided). In contrast, multi-scale hexagonal patterns emerged in the Reverse-replay condition

(Fig.4h & Fig.S2b, mean grid score= 1.32 / 1.28 / 1.39 / 1.32, for Mod I / II / III / IV, respectively. $p < 0.05$, initial threshold, $p < 0.05$; corrected for multiple comparisons), showing significantly higher overall grid score than those in the No-replay condition across grid scales (Fig.4h, $t(15) = 8.85$, $p<0.001$, two-sided). In summary, these results demonstrate a potential critical role of reverse replay in maintaining the newly formed receptive fields of hexagonal patterns during pattern translation, particularly for high resolution representation.

Discussion

The present study utilized CAN models to investigate the role of experience replay in facilitating the hexagonal pattern formation of grid cells. We found that reverse experience replay, as opposed to no replay, forward replay, or shuffled-experience replay, promoted the formation of multi-scale hexagonal patterns. This effect was particularly effective in enhancing the spatial regularity of small-scale hexagonal patterns. Thus, these findings presumably reflect the role of place cell replay in constructing high-resolution metrics of grid cells (Schuck and Niv, 2019). Further analyses revealed that the efficiency of reverse replay in hexagonal pattern formation was influenced by the interplay of grid scales and the amount of experience (i.e., limited versus extended environmental exploration). This finding demonstrated that regular hexagonal pattern formation depends on balancing the spatial and temporal demands of pattern generation. Specifically, reverse replay prevents the disruption of generated receptive fields caused by the edge effects during wave propagation by using representational transfer, which folds space into a grid in a periodic manner. This computational mechanism might be the key to achieving infinite space tessellation with a finite number of neurons.

The formation of abstract knowledge has been strongly associated with both hippocampal experience replay (Wu and Foster, 2014; Liu et al., 2019; Liu et al., 2021; Kurth-Nelson et al., 2023) and entorhinal grid cells (McNaughton et al., 2006; Behrens et al., 2018; Bellmund et al., 2019; Bellmund et al., 2020; Peer et al., 2021; Whittington et al., 2022). The present study provides computational evidence supporting their potential link and offers two key implications. First, the mechanism underlying the formation of small to large hexagonal patterns may not follow a linear progression but rather a categorical distinction. Consistent with the reaction-diffusion model, where Turing-instability varies non-linearly as a function of spatial frequency (Yang et al., 2004), our results showed that large scale hexagonal patterns spontaneously emerged independent of experience replay, whereas small scale hexagonal patterns depended on experience replay. Anatomically, the spatial scales of both entorhinal grid cell and hippocampal place cells decrease along the anteroposterior (ventral-dorsal) axis, with the posterior area, a particularly common recording site for experience replay (Carr et al., 2012; Pfeiffer & Foster, 2013; Ambrose et al., 2016; Gillespie et al., 2021), representing fine-grained experiences compared to the anterior area, which encodes coarse experiences (Hafting et al., 2005; Stensola et al., 2012; Strange et al., 2014; Schiller et al., 2015). For instance, hippocampal sharp wave ripples, which facilitate experience

replay, are typically characterized by transient high-frequency oscillations for precise location coding (Buzsáki, 2015). These findings align well with our observations that small-scale hexagonal pattern formation relies on experience replay for fine-grained spatial representation.

Another implication of the present work is that the rapid formation of high-resolution hexagonal metrics is likely associated with hippocampal experience replay. CAN models have been extensively used to simulate hexagonal patterns (Hafting et al., 2005; Burak and Fiete, 2009; Couey et al., 2013; Kang and Balasubramanian, 2019; Khona et al., 2021; Sorscher et al., 2023). However, simulations of regular hexagonal patterns have typically been based on saturated environmental exploration, assuming that animal's foraging behavior involves visiting a large number of spatial locations and directions. Interestingly, grid cell activity has been observed in one-dimensional linear track (Yoon et al., 2016) and circular track (Jacob et al., 2019), despite the constraints that these experimental environments impose on direction or location. Moreover, grid cell activity has been elicited by eye movements during visual attention tasks (Nau et al., 2018; Killian & Buffalo, 2018; Staudigl et al., 2018; Julian et al., 2018; Wilming et al., 2018), demonstrating the capacity of grid cell to map visual space. For instance, in Staudigl (2018), grid cells mapped eye movements during freely viewing 100 indoor and 100 outdoor images. Intuitively, high-resolution hexagonal metrics are required to meet the task demands of identifying small objects within rich image textures. These findings demonstrate that the hexagonal patterns of grid cells can be rapidly formed under spatial and temporal constraints during environmental exploration.

In addition to the implications of the present study, our results can not fully account for the biological realism and plausibility of the hippocampal–entorhinal circuit. One limitation is that we selectively simulated the unidirectional impacts of place cell replay on the formation of hexagonal patterns. Consequently, our explanations were based on the predefined location representations of place cells. However, grid cells and place cells are known to function as a complementary and interacting system that supports the reliable coding of external space (Solstad et al., 2006; Brun et al., 2008; Bush et al., 2014; Bush et al., 2015; Bicanski & Burgess, 2019). Therefore, future studies should explore the bidirectional interactions between the hexagonal patterns of grid cells and place cell replay. Another aspect concerns the maturation of grid cells and place cell replay observed in biological system. While there is some overlap in their maturation around postnatal day 20 (Wills & Cacucci, 2014; Farooq & Dragoi, 2019), previous studies have indicated that grid cell activity

can be observed in rats as young as P16 (Langston et al., 2010; Wills et al., 2010), despite the irregularity of hexagonal patterns at this stage. One possible explanation is that these early grid-like cells represent coarse spatial representations that are independent of hippocampal experience replay. Future research should address these unsolved issues by modelling a unified hippocampal–entorhinal circuit to investigate the simultaneous development of place cells and grid cells.

Materials and Methods

Simulation of multi-scale hexagonal pattern

Multi-scale hexagonal patterns of grid cell were simulated on an n-by-n-pixel square representational space ξ using CAN model (Fuhs and Touretzky, 2006; Burak and Fiete, 2009; Couey et al., 2013; Kang and Balasubramanian, 2019; Torch Version 1.13, Python version 3.9), where n=45 pixels. Each pixel i in the space, representing a spatial location (x, y), corresponded to a place cell i, which was connected to a downstream grid cell i at each spatial scale (Bonnevie et al., 2013; Rennó-Costa and Tort, 2017). Specifically, a series of "walking" experience were included in a single CAN simulation. Each experience, defined by numeric spatial movements with a movement step size λ of 3 pixels in a given spatial direction θ, was designed to activate a sequence of place cells. These place cell activities generated a displacement vector signal v at each location during CAN pattern translation, indicating which grid cell would be activated when approaching adjacent locations (Equation 1).

$$v = \lambda \cdot (\cos(\theta), \sin(\theta)) \tag{1}$$

The procedure for synaptic plasticity updates during CAN pattern translation is illustrated in Equation 2. The membrane voltage ξ of grid cell i, simulated as a two-dimensional n-by-n matrix, was initialized at zero. Upon receiving place cell activity, ξ_i was scaled to simulate the firing rate f_i of the neuron if the voltage strength exceeded the threshold η (i.e., $\eta = 0$; Equation 3; see also table S1). Otherwise, ξ_i was inhibited to zero using a nonlinear transfer function at that location. Thus, all active location representations of grid cell i that surpassed the threshold η across the space were identified. These firing rates were weighted by the predefined excitatory and inhibitory matrix W_{ij}, which represents the periodic connection strengths of grid cell i with grid cells j that encoded these locations (Fig.S4). This process formed the conjunctive activity update for ξ by summing the weighted firing rates of grid cells j. The procedure was repeated over spatial movements until the number of movements within a simulation reached the predefined limit (1200 movements). The time constant τ was set to 10 ms. The noise ε in the pattern displacement vector v was applied in the "extended exploration" condition, while ε was set to zero in the "limited exploration" condition.

$$\tau \frac{d\xi_i}{dt} = -\xi_i + \sum_j W_{ij} f_j + v_i + \varepsilon \tag{2}$$

$$f_i = \begin{cases} \sqrt{\xi_i}, & \xi_i > \eta \\ 0, & \xi_i \leq \eta \end{cases} \tag{3}$$

The recurrent weight W, represented as a two-dimensional symmetric matrix, was simulated using the representational oscillatory interference of elementary neurons proposed by the oscillatory interference model (Fig.S4 & Table.S1; Burgess et al., 2007; Burgess, 2008; Bush & Burgess, 2014). This model hypothesizes the involvement of velocity-controlled oscillator neurons (VCO), whose burst-firing strength varies with spatial directions and movement speed, such that displacement in a given direction produces band-like or stripe-like firing patterns. Specifically, the burst-firing maps of VCOs in direction θ are formalized as $\cos(\omega(\nu_x X + \nu_y Y))$ (Equation 4), where ν_x and ν_y, derived from $\cos(\theta)$ and $\sin(\theta)$, determines the preferred displacement direction of the activity gradient $\nu_x X + \nu_y Y$. Here, X and Y denote two-dimensional matrices in which each element represents the x- and y-coordinate, respectively. At each location (x, y), a recurrent weight $W_{(x,y)}$ was generated by linearly summing the burst-firing maps of VCOs at spatial frequency ω, representing all possible directions radiating from (x, y). The spatial frequency ω, defined in Equation 5, depends on grid scales σ, which represents Euclidean distance between two adjacent periodic activity peaks and is positively related to receptive field size. Grid scale of 11, 15, 22, 30 pixels, equivalent to 24%, 33%, 49%, and 67% of the representational space size, respectively, were selected for simulating the multi-scale hexagonal patterns based on a grid ratio of $\sqrt{2}$, as suggested by previous studies (Stemmler et al., 2015; Wei et al., 2015; Kang and Balasubramanian, 2019). For instance, the grid scale σ = 30 (i.e., 30 pixels) corresponds to a relatively lower spatial frequency compared to σ = 11. These grid scales were treated as independent during CAN simulation.

$$W_{(x,y)} = \sum_{\theta=0}^{\infty} \alpha \cos(\omega(\nu_x X + \nu_y Y)) \tag{4}$$

$$\omega = 2pi/\sigma \tag{5}$$

The periodic repeating pattern of grid cells are known to reside on torus topology (Samsonovich and McNaughton, 1997; McNaughton et al., 2006; Knierim and Zhang, 2012; Khona & Fiete, 2022; Gardner et al., 2022; Sorscher et al., 2023). This topology is conceptualized by connecting the opposite edges of a square representational space, implying that the periodic activity of grid cells transcends boundary effects when moving along a straight line in the space. To simulate this periodic boundary condition, we assumed that the periodic boundaries are a neural characteristic of adult-like grid cells. These neurons should exhibit significant grid scores relative to the shuffled threshold, ensuring that the regular periodicity of hexagonal patterns maintains accurate location displacements at opposite edge when the CAN model approaches to boundary. For this simulation, we extracted the grid orientation, estimated using the autocorrelation maps of grid cells at each movement step (Fig.S5). With grid orientation and grid scale determined, we interpolated grid activity at each edge location based on adjacent grid activity along the three main axes of the hexagonal pattern. This method predicted when and where specific phases of the hexagonal pattern would appear at the edges, based on the known grid scale and orientation.

Simulation of hippocampal replay

To examine the impact of experience replay on the regularity of multi-scale hexagonal patterns generated by CAN, we intentionally manipulated the sequential activity of place cells at the "decision point" that mimics animal's decision point (denoted by the red dots in Fig.2a, e-g). The place cell activity represents the experience of sequential visited locations with either reverse, forward, or shuffled spatial directions relative to each of actual past experience. The No-replay condition was used as control, where no additional activity input of place cell was applied to CAN simulation. In the Forward-/Reverse-replay condition, CAN received the sequential activity of place cells indicating the identical/reverse directions prior to/next to the actual movements, respectively. The Shuffled-replay condition examines the necessity of the spatial and temporal structure of past experience during experience replay, where the sequential activity of place cells from past experiences were shuffled in temporal domain before sending to CAN, and were reversely replayed at the "decision point" during pattern translation. Each simulation of experience replay consisted of a series of "walking" experiences, each of which was randomly paired with either 5-, 10-, or 15-movement locations along the spatial direction determined by the sequential activity of place cells. The total number of movements in each simulation was constrained to 1200

movements. The movement trajectories of CAN were finally projected on a squared space created by Unity (Unity Technologies, San Francisco) for visualization purpose.

In addition to the type of replay, we examined the impact of amount of experience of place cell replay on multi-scale hexagonal pattern formation during limited and extended exploration. The limited exploration experiment aims to examine the possibility of the rapid formation of grid-like representational space observed during eye movements (Nau et al., 2018; Killian & Buffalo, 2018; Staudigl et al., 2018; Julian et al., 2018; Wilming et al., 2018) and the movments in one-dimensional linear and circular track (Yoon et al., 2016; Jacob et al., 2019). We constrained the movement experience to three spatial directions, each separated by 45° (70°,115°, and 160° with 0° pointing towards East). Each "walking" experience was randomly assigned with one out of the three spatial direction. Meanwhile, the length of movements within each experience remained unchanged (i.e., either 5-, 10-, or 15-locations). This design excluded the possibility of the confounding effect that the "walking" direction is opposite to actual experience, which is identical to the impact of reverse replay, although the walking experiences with reversed movement direction have been commonly involved during saturated environmental exploration (Hafting et al., 2005; Burak and Fiete, 2009; Couey et al., 2013; Kang and Balasubramanian, 2019; Khona et al., 2021; Sorscher et al., 2023). To ensure the robustness of limited exploration simulation, each type of experience replay was independently simulated 15 times before group-level analysis.

Three "extended exploration" experiments were conducted to examine the impact of reverse replay on multi-scale hexagonal pattern formation compared to that of no replay under a large number of walking directions or locations. Firstly, we examined the impact of AE and grid scale on the regularity of hexagonal patterns (i.e., how grid score changes as a function of AEs and grid scales). A total of 29 AEs, ranged from 2 to 30 locations with a step size of 1, and a total of 20 grid scales, ranged from 11 to 30 pixels (Table 1), were prepared. This resulted in a total of 1160 simulations with 15 simulations for each AE-grid scale pair. The impact of AEs and grid scales on hexagonal pattern formation was assessed by the slope $-\frac{1}{k}$ of exponential decay function $ae^{(\frac{-AE}{k})}$, which was calculated in each grid scale and type of replay, and predicts how fast grid score reaches the significance threshold within the simulation given AE, grid scale and type of replay. The slopes were first linearized via log transformation and was subsequently fitted by the curve_fit function of scipy package (version 1.9.3). Secondly, an open-source dataset (Fig.4a; Hafting et al., 2005; https://www.ntnu.edu/kavli/research/grid-cell-data) was used to examine the

multi-scale hexagonal regularity during extended exploration in the No-replay condition. The datasets included a large number of movement trajectories of rats as they collected randomly scattered pieces of food in an open square-shaped environment, and thus offering diversely-distributed movement directions ranged from 0° - 360°. The total number of locations of rat movements were down-sampled to 1200. Finally, we examined the impact of reverse replay on hexagonal pattern formation under a large number of walking locations and a constrained number of walking directions. In this experiment, the "walking" experiences were constrained by one out of eight predefined global directions, each 45° apart (Fig.4d; 0°, 45°, 90°, 135°, 180°, 225°, 270°, and 315°), plus an random noise ϵ between -90° to 90°. This resulted in a large number of walking locations with walking directions constrained in 180° (Fig.4f), thus excluding the possibility of the replay direction opposite to actual experience. To ensure the robustness of simulations, 16 simulations were independently performed (Fig.4d; each global direction was repeated twice) before group-level analysis.

<u>Validation of grid regularity</u>

The spatial regularity of hexagonal patterns, as indexed by grid score, was computed with the following procedures introduced previously (Sargolini et al., 2006; Barry & Burgess, 2017). The spatial autocorrelation of each hexagonal pattern was estimated by Equation 6, which calculated Pearson's product moment correlation coefficient for each representational location (x, y) of hexagonal pattern based on the neural activity $\lambda(x, y)$ and the spatial lags τ_x and τ_y over n locations. The autocorrelogram was further rotated by 30°, 60°, 90°, 120°, and 150°, the similarity between the rotated autocorrelogram and the original autocorrelogram was assessed by Pearson correlation. Grid score was finally derived by subtracting the highest similarity of 30°, 90° and 150° from the minimum similarity of 60° and 120°.

$$r(\tau_x,\tau_y)=\frac{n\sum\lambda(x,y)\lambda(x-\tau_x,y-\tau_y)-\sum\lambda(x,y)\lambda(x-\tau_x,y-\tau_y)}{\sqrt{n\sum\lambda(x,y)^2(\sum\lambda(x,y))^2}\sqrt{n\sum\lambda(x-\tau_x,y-\tau_y)^2(\sum\lambda(x-\tau_x,y-\tau_y))^2}} \quad (6)$$

To assess the hexagonal pattern regularity of grid cell population, we followed the analytical pipeline of persistent cohomology (Ghrist, 2008; Gardner et al., 2022), using the package Ripser++ (Version 1.1.2) and umap-learn (Version 0.5.7) (Zhang et al., 2020; Bauer, 2021). For each grid scale, persistent cohomology was used to identify the potential toroidal

structure in the population activity of grid cells, which has been shown to exist in the grid cell population of biological brain (Gardner et al., 2022). Specifically, the high-dimension representation of CAN-generated grid cells were first reduced to six dimensions using principal component analysis (PCA). This linear embedding preserved the hexagonal structures and mitigated the "curse of dimensionality". Subsequently, a second nonlinear dimensionality reduction step was applied, reducing the data to three dimensions for point-cloud visualization of grid cell activity. This step utilized UMAP (Uniform Manifold Approximation and Projection for Dimension Reduction) with the following hyperparameters: 'n_components'=3, metric='cosine', 'min_dist'=0.8, 'init'=' spectral' (Gardner et al., 2022). In the persistence analysis, cohomology was used to detect the global topological structure of the Z-transformed three-dimensional embedding, characterized by a toroidal structure in Euclidean space. In doing so, each point in the point cloud were replaced with a ball of infinitesimal radius. Upon increasing the radius of balls, the balls are gradually expanded to form certain global structure with holes of different dimensions. The lifespans of the balls, indicated by the range of radii from when they appeared to when they disappeared, were represented by the lengths of the bars. (i.e., barcodes). A toroidal structure is expected to have one 0D hole (the connected object[i.e., entire torus]), two 1D holes (the inner and outer hole of torus), and one 2D hole (the cavity in the interior of torus). Therefore, the hexagonal patterns of CAN-generated grid cells were considered regular if the expected number of holes are detected and persisted for a sufficiently long duration during ball radius expansion, compared to the significance threshold derived from permutation. To minimize the noise of dimensionality reduction caused by the imbalanced representation of spatial locations given the arbitrary size of grid cell population in the 45-by-45-pixel representational space and grid scales, not all CAN-generated grid cells were used in the persistent cohomology analysis. Instead, for each spatial scale, we selected a population of grid cell to ensure that each location was represented by an approximately equivalent number of receptive fields (Fiete et al., 2008), considering grid orientation and grid scales. As a result, groups of 110 neurons, 117 neurons, 247 neurons, and 319 neurons were selected for grid Mod I, II, III, and IV, respectively.

Statistics

To quantify the significance of hexagonal pattern regularity, grid score distribution was created using field-shuffling permutation (Fig.S9; Krupic et al., 2012). The significance threshold

of grid scores was derived from the distribution. Specifically, the hexagonal patterns generated in the Reverse-replay condition, which produced on average the highest grid scores across the conditions, were used for field-shuffling permutation. The original spatial structures of each hexagonal pattern were shuffled by randomly changing the positions of receptive fields 1000 times with the local structure (the shape of receptive fields) preserved. The uncorrected threshold was determined by the 99th percentile of the grid scores of shuffled hexagonal patterns. The significant threshold corrected for multiple comparisons was further determined by the 95th percentile of the uncorrected-threshold distribution of hexagonal pattern population. The same procedure was used for persistent cohomology analysis, where the uncorrected threshold and the corrected threshold for multiple comparisons were determined by the 99th and 95th percentiles of the random distribution of barcodes, estimated based on the shuffled activity patterns of the receptive field, respectively. The significance thresholds were finally averaged across grid scales. The grid score differences between small scale (Mod I & Mod II) and large scale (Mod III & Mod IV) hexagonal patterns were examined using two sample t-test, two-tailed. The impact of the type of experience replay, amount of experience, and grid scales on grid scores were examined using ANOVA. Pearson correlation was used to examine the linear relationship of grid scores' decay slope with grid scale and amount of experience, respectively.

Acknowledgments

We thank Dr. Yunzhe Liu, Dr. Olaf Sporns, and Dr. Dietmar Plenz for providing valuable comments on the manuscript. This work was supported by the National Key R&D Program of China [2020AAA0105200], China Postdoctoral Science Foundation [2022M710470], Beijing Municipal Science & Technology Commission & Administrative Commission of Zhongguancun Science Park [Z221100002722012], Tsinghua University Guoqiang Institute [2020GQG1016], and Beijing Academy of Artificial Intelligence (BAAI).

Author Contributions

B.Z. and J.L. conceived the study; B.Z. built the computational model and performed the analysis; L.M. provided valuable advice and assistance; B.Z. and J.L. wrote the paper.

Conflict of interest

None declared.

Data availability

Raw data reported in the present study are available from the corresponding author upon reasonable request.

Code availability

The .NET code for generating the virtual environment and the Python code for simulating the formation of multi-scale hexagonal patterns of grid cells are available at https://github.com/ZHANGneuro/Hippocampal-replay-facilitates-the-formation-of-entorhinal-grid-cells.

Reference

Ambrose, R. E., Pfeiffer, B. E., & Foster, D. J. (2016). Reverse replay of hippocampal place cells is uniquely modulated by changing reward. Neuron, 91(5), 1124-1136.

Barry, C., & Burgess, N. (2017). To be a Grid Cell: Shuffling procedures for determining "Gridness". BioRxiv, 230250.

Brun, V. H., Leutgeb, S., Wu, H. Q., Schwarcz, R., Witter, M. P., Moser, E. I., & Moser, M. B. (2008). Impaired spatial representation in CA1 after lesion of direct input from entorhinal cortex. Neuron, 57(2), 290-302.

Burak, Y., & Fiete, I. R. (2009). Accurate path integration in continuous attractor network models of grid cells. PLoS computational biology, 5(2), e1000291.

Barry, C., Ginzberg, L. L., O'Keefe, J., & Burgess, N. (2012). Grid cell firing patterns signal environmental novelty by expansion. Proceedings of the National Academy of Sciences, 109(43), 17687-17692.

Behrens, T. E., Muller, T. H., Whittington, J. C., Mark, S., Baram, A. B., Stachenfeld, K. L., & Kurth-Nelson, Z. (2018). What is a cognitive map? Organizing knowledge for flexible behavior. Neuron, 100(2), 490-509.

Burgess, N., Maguire, E. A., & O'Keefe, J. (2002). The human hippocampus and spatial and episodic memory. Neuron, 35(4), 625-641.

Burgess, N., Barry, C., & O'keefe, J. (2007). An oscillatory interference model of grid cell firing. Hippocampus, 17(9), 801-812.

Burgess, N. (2008). Grid cells and theta as oscillatory interference: theory and predictions. Hippocampus, 18(12), 1157-1174.

Bonnevie, T., Dunn, B., Fyhn, M., Hafting, T., Derdikman, D., Kubie, J. L., ... & Moser, M. B. (2013). Grid cells require excitatory drive from the hippocampus. Nature neuroscience, 16(3), 309-317.

Bush, D., Barry, C., & Burgess, N. (2014). What do grid cells contribute to place cell firing?. Trends in neurosciences, 37(3), 136-145.

Buzsáki, G. (2015). Hippocampal sharp wave-ripple: A cognitive biomarker for episodic memory and planning. Hippocampus, 25(10), 1073-1188.

Bush, D., & Burgess, N. (2014). A hybrid oscillatory interference/continuous attractor network model of grid cell firing. Journal of Neuroscience, 34(14), 5065-5079.

Bush, D., Barry, C., Manson, D., & Burgess, N. (2015). Using grid cells for navigation. Neuron, 87(3), 507-520.

Bicanski, A., & Burgess, N. (2019). A computational model of visual recognition memory via grid cells. Current Biology, 29(6), 979-990.

Bellmund, J. L., Deuker, L., & Doeller, C. F. (2019). Mapping sequence structure in the human lateral entorhinal cortex. elife, 8, e45333.

Bellmund, J. L., De Cothi, W., Ruiter, T. A., Nau, M., Barry, C., & Doeller, C. F. (2020). Deforming the metric of cognitive maps distorts memory. Nature human behaviour, 4(2), 177-188.

Bauer, U. (2021). Ripser: efficient computation of Vietoris–Rips persistence barcodes. Journal of Applied and Computational Topology, 5(3), 391-423.

Couey, J. J., Witoelar, A., Zhang, S. J., Zheng, K., Ye, J., Dunn, B., ... & Witter, M. P. (2013). Recurrent inhibitory circuitry as a mechanism for grid formation. Nature neuroscience, 16(3), 318-324.

Carr, M. F., Jadhav, S. P., & Frank, L. M. (2011). Hippocampal replay in the awake state: a potential substrate for memory consolidation and retrieval. Nature neuroscience, 14(2), 147-153.

Carr, M. F., Karlsson, M. P., & Frank, L. M. (2012). Transient slow gamma synchrony underlies hippocampal memory replay. Neuron, 75(4), 700-713.

Diba, K., & Buzsáki, G. (2007). Forward and reverse hippocampal place-cell sequences during ripples. Nature neuroscience, 10(10), 1241-1242.

Fiete, I. R., Burak, Y., & Brookings, T. (2008). What grid cells convey about rat location. Journal of Neuroscience, 28(27), 6858-6871.

Fuhs, M. C., & Touretzky, D. S. (2006). A spin glass model of path integration in rat medial entorhinal cortex. Journal of Neuroscience, 26(16), 4266-4276.

Foster, D. J., & Wilson, M. A. (2006). Reverse replay of behavioural sequences in hippocampal place cells during the awake state. Nature, 440(7084), 680-683.

Farooq, U., & Dragoi, G. (2019). Emergence of preconfigured and plastic time-compressed sequences in early postnatal development. Science, 363(6423), 168-173.

Gardner, R. J., Hermansen, E., Pachitariu, M., Burak, Y., Baas, N. A., Dunn, B. A., ... & Moser, E. I. (2022). Toroidal topology of population activity in grid cells. Nature, 602(7895), 123-128.

Gillespie, A. K., Maya, D. A. A., Denovellis, E. L., Liu, D. F., Kastner, D. B., Coulter, M. E., ... & Frank, L. M. (2021). Hippocampal replay reflects specific past experiences rather than a plan for subsequent choice. Neuron, 109(19), 3149-3163.

Ghrist, R. (2008). Barcodes: the persistent topology of data. Bulletin of the American Mathematical Society, 45(1), 61-75.

Hafting, T., Fyhn, M., Molden, S., Moser, M. B., & Moser, E. I. (2005). Microstructure of a spatial map in the entorhinal cortex. Nature, 436(7052), 801-806.

Hägglund, M., Mørreaunet, M., Moser, M. B., & Moser, E. I. (2019). Grid-cell distortion along geometric borders. Current Biology, 29(6), 1047-1054.

Jacob, P. Y., Capitano, F., Poucet, B., Save, E., & Sargolini, F. (2019). Path integration maintains spatial regularity of grid cell firing in a 1D circular track. Nature Communications, 10(1), 1-13.

Julian, J. B., Keinath, A. T., Frazzetta, G., & Epstein, R. A. (2018). Human entorhinal cortex represents visual space using a boundary-anchored grid. Nature neuroscience, 21(2), 191-194.

Killian, N. J., & Buffalo, E. A. (2018). Grid cells map the visual world. Nature neuroscience, 21(2), 161-162.

Khona, M., & Fiete, I. R. (2022). Attractor and integrator networks in the brain. Nature Reviews Neuroscience, 1-23.

Kang, L., & Balasubramanian, V. (2019). A geometric attractor mechanism for self-organization of entorhinal grid modules. Elife, 8.

Krupic, J., Burgess, N., & O'Keefe, J. (2012). Neural representations of location composed of spatially periodic bands. Science, 337(6096), 853-857.

Knierim, J. J., & Zhang, K. (2012). Attractor dynamics of spatially correlated neural activity in the limbic system. Annual review of neuroscience, 35, 267-285.

Kurth-Nelson, Z., Behrens, T., Wayne, G., Miller, K., Luettgau, L., Dolan, R., ... & Schwartenbeck, P. (2023). Replay and compositional computation. Neuron, 111(4), 454-469.

Khona, M., Chandra, S., & Fiete, I. (2021). Emergence of robust global modules from local interactions and smooth gradients. bioRxiv, 2021-10.

Langston, R. F., Ainge, J. A., Couey, J. J., Canto, C. B., Bjerknes, T. L., Witter, M. P., ... & Moser, M. B. (2010). Development of the spatial representation system in the rat. Science, 328(5985), 1576-1580.

Liu, Y., Dolan, R. J., Kurth-Nelson, Z., & Behrens, T. E. (2019). Human replay spontaneously reorganizes experience. Cell, 178(3), 640-652.

Liu, Y., Mattar, M. G., Behrens, T. E., Daw, N. D., & Dolan, R. J. (2021). Experience replay is associated with efficient nonlocal learning. Science, 372(6544), eabf1357.

Larkin, M. C., Lykken, C., Tye, L. D., Wickelgren, J. G., & Frank, L. M. (2014). Hippocampal output area CA1 broadcasts a generalized novelty signal during an object-place recognition task. Hippocampus, 24(7), 773-783.

Moser, E. I., Moser, M. B., & McNaughton, B. L. (2017). Spatial representation in the hippocampal formation: a history. Nature neuroscience, 20(11), 1448-1464.

McNaughton, B. L., Battaglia, F. P., Jensen, O., Moser, E. I., & Moser, M. B. (2006). Path integration and the neural basis of the 'cognitive map'. Nature Reviews Neuroscience, 7(8), 663-678.

Mattar, M. G., & Daw, N. D. (2018). Prioritized memory access explains planning and hippocampal replay. Nature neuroscience, 21(11), 1609-1617.

Nau, M., Schröder, T. N., Bellmund, J. L., & Doeller, C. F. (2018). Hexadirectional coding of visual space in human entorhinal cortex. Nature neuroscience, 21(2), 188-190.

Nour, M. M., Liu, Y., Arumuham, A., Kurth-Nelson, Z., & Dolan, R. J. (2021). Impaired neural replay of inferred relationships in schizophrenia. Cell, 184(16), 4315-4328.

Ólafsdóttir, H. F., Carpenter, F., & Barry, C. (2016). Coordinated grid and place cell replay during rest. Nature neuroscience, 19(6), 792-794.

Pfeiffer, B. E., & Foster, D. J. (2013). Hippocampal place-cell sequences depict future paths to remembered goals. Nature, 497(7447), 74-79.

Pfeiffer, B. E. (2020). The content of hippocampal “replay”. Hippocampus, 30(1), 6-18.

Peer, M., Brunec, I. K., Newcombe, N. S., & Epstein, R. A. (2021). Structuring knowledge with cognitive maps and cognitive graphs. Trends in cognitive sciences, 25(1), 37-54.

Rolls, E. T., Stringer, S. M., & Elliot, T. (2006). Entorhinal cortex grid cells can map to hippocampal place cells by competitive learning. Network: Computation in Neural Systems, 17(4), 447-465.

Rennó-Costa, C., & Tort, A. B. (2017). Place and grid cells in a loop: implications for memory function and spatial coding. Journal of Neuroscience, 37(34), 8062-8076.

Suh, J., Foster, D. J., Davoudi, H., Wilson, M. A., & Tonegawa, S. (2013). Impaired hippocampal ripple-associated replay in a mouse model of schizophrenia. Neuron, 80(2), 484-493.

Schiller, D., Eichenbaum, H., Buffalo, E. A., Davachi, L., Foster, D. J., Leutgeb, S., & Ranganath, C. (2015). Memory and space: towards an understanding of the cognitive map. Journal of Neuroscience, 35(41), 13904-13911.

Strange, B. A., Witter, M. P., Lein, E. S., & Moser, E. I. (2014). Functional organization of the hippocampal longitudinal axis. Nature Reviews Neuroscience, 15(10), 655-669.

Samsonovich, A., & McNaughton, B. L. (1997). Path integration and cognitive mapping in a continuous attractor neural network model. Journal of Neuroscience, 17(15), 5900-5920.

Solstad, T., Moser, E. I., & Einevoll, G. T. (2006). From grid cells to place cells: a mathematical model. Hippocampus, 16(12), 1026-1031.

Sargolini, F., Fyhn, M., Hafting, T., McNaughton, B. L., Witter, M. P., Moser, M. B., & Moser, E. I. (2006). Conjunctive representation of position, direction, and velocity in entorhinal cortex. Science, 312(5774), 758-762.

Schuck, N. W., & Niv, Y. (2019). Sequential replay of nonspatial task states in the human hippocampus. Science, 364(6447), eaaw5181.

Stemmler, M., Mathis, A., & Herz, A. V. (2015). Connecting multiple spatial scales to decode the population activity of grid cells. Science Advances, 1(11), e1500816.

Staudigl, T., Leszczynski, M., Jacobs, J., Sheth, S. A., Schroeder, C. E., Jensen, O., & Doeller, C. F. (2018). Hexadirectional modulation of high-frequency electrophysiological activity in the human anterior medial temporal lobe maps visual space. Current Biology, 28(20), 3325-3329.

Schacter, D. L., Addis, D. R., & Buckner, R. L. (2007). Remembering the past to imagine the future: the prospective brain. Nature reviews neuroscience, 8(9), 657-661.

Stensola, H., Stensola, T., Solstad, T., Frøland, K., Moser, M. B., & Moser, E. I. (2012). The entorhinal grid map is discretized. Nature, 492(7427), 72-78.

Sorscher, B., Mel, G., Ganguli, S., & Ocko, S. (2019). A unified theory for the origin of grid cells through the lens of pattern formation. Advances in neural information processing systems, 32.

Sorscher, B., Mel, G. C., Ocko, S. A., Giocomo, L. M., & Ganguli, S. (2023). A unified theory for the computational and mechanistic origins of grid cells. Neuron, 111(1), 121-137.

Tulving, E., & Markowitsch, H. J. (1998). Episodic and declarative memory: role of the hippocampus. Hippocampus, 8(3), 198-204.

Tolman, E. C. (1948). Cognitive maps in rats and men. Psychological review, 55(4), 189.

Wills, T. J., Cacucci, F., Burgess, N., & O'Keefe, J. (2010). Development of the hippocampal cognitive map in preweanling rats. science, 328(5985), 1573-1576.

Wu, X., & Foster, D. J. (2014). Hippocampal replay captures the unique topological structure of a novel environment. Journal of Neuroscience, 34(19), 6459-6469.

Wills, T. J., & Cacucci, F. (2014). The development of the hippocampal neural representation of space. Current opinion in neurobiology, 24, 111-119.

Wei, X. X., Prentice, J., & Balasubramanian, V. (2015). A principle of economy predicts the functional architecture of grid cells. Elife, 4, e08362.

Wilming, N., König, P., König, S., & Buffalo, E. A. (2018). Entorhinal cortex receptive fields are modulated by spatial attention, even without movement. Elife, 7, e31745.

Whittington, J. C., McCaffary, D., Bakermans, J. J., & Behrens, T. E. (2022). How to build a cognitive map. Nature neuroscience, 25(10), 1257-1272.

Yoon, K., Lewallen, S., Kinkhabwala, A. A., Tank, D. W., & Fiete, I. R. (2016). Grid cell responses in 1D environments assessed as slices through a 2D lattice. Neuron, 89(5), 1086-1099.

Yang, L., Zhabotinsky, A. M., & Epstein, I. R. (2004). Stable squares and other oscillatory Turing patterns in a reaction-diffusion model. Physical review letters, 92(19), 198303.

Zhang, S., Xiao, M., & Wang, H. (2020). GPU-accelerated computation of Vietoris-Rips persistence barcodes. arXiv preprint arXiv:2003.07989.

Supplemental Material

“Experience replay facilitates the rapid formation of multi-scale hexagonal patterns of grid cells”

Bo Zhang, Lei Ma, and Jia Liu

Figure S1. Multi-scale hexagonal patterns generated by CAN models with reverse replay. For each scale, 24 grid cell samples were shown as example and were sorted by phase along the horizontal and vertical axis.

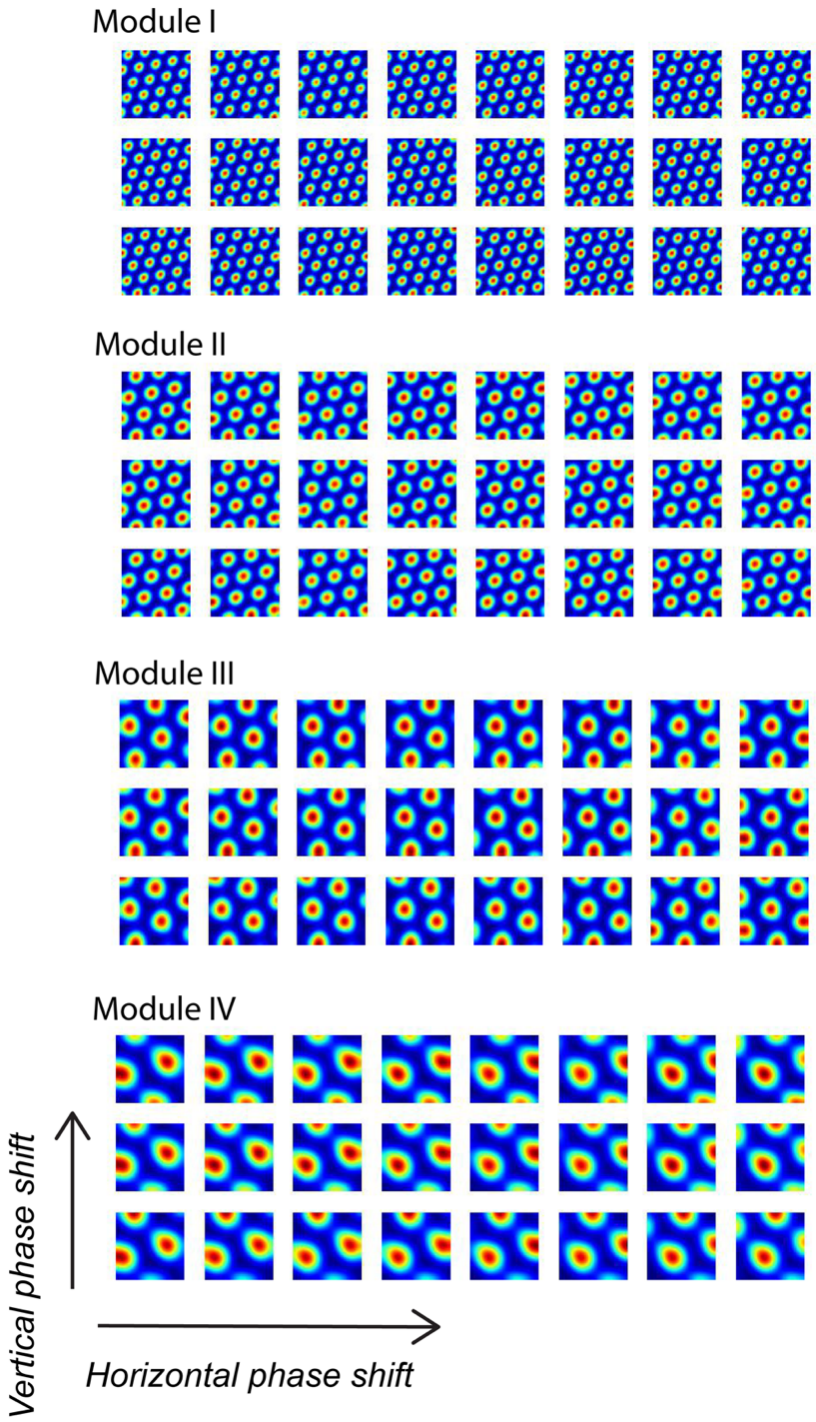

Figure S2. Impact of experience replay on grid scores. 15 and 16 independent simulations that correspond to Fig.2 and 4 were performed for (a) and (b), respectively.

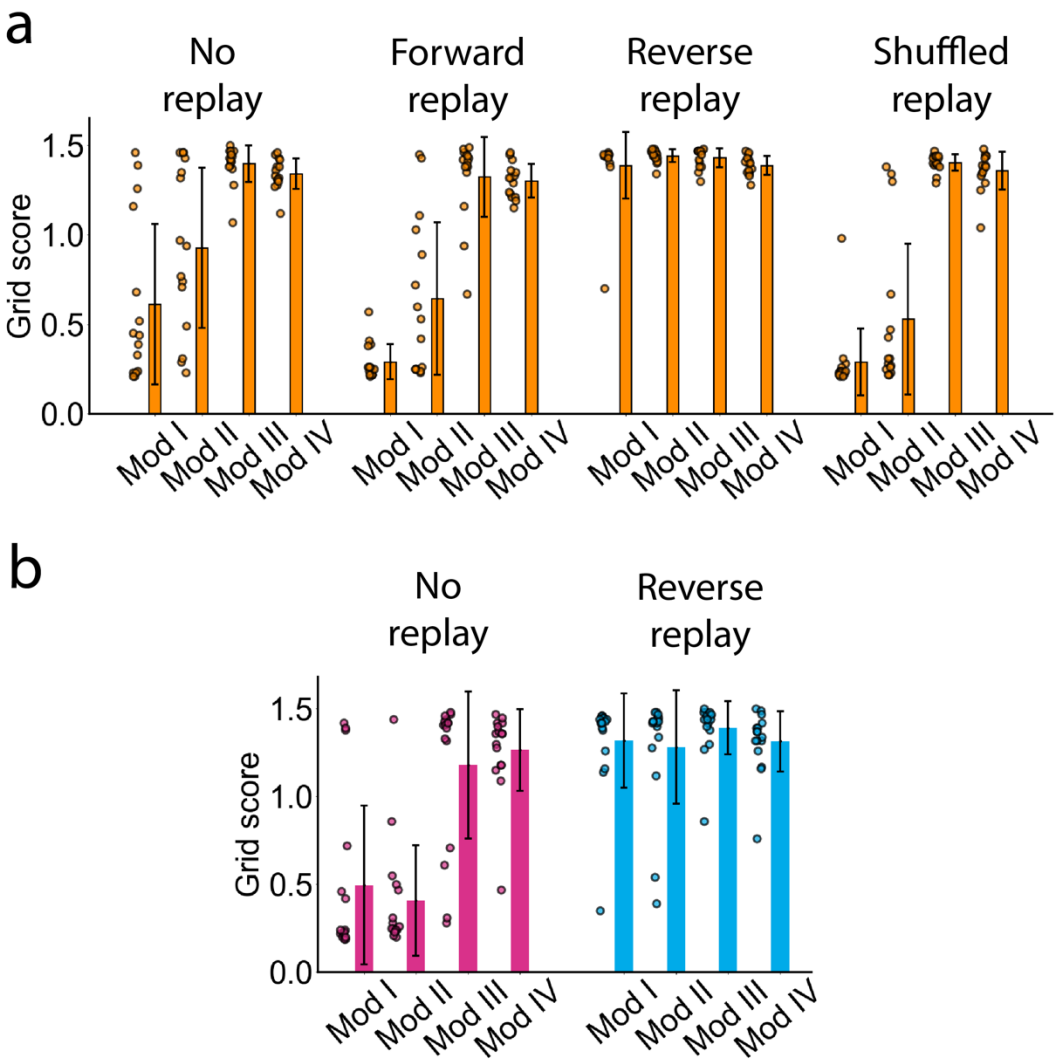

Figure S3. Toroidal structures at each grid scale revealed from population activity of CAN-generated grid cells. Dimensionality-reduced grid cell activities (right column), colored by the first principal component, were derived based on CAN models under the Reverse-replay condition. In the barcodes (left column), the top 30 holes (green bars) with the longest lifespans (radii of balls) are shown for the 0D hole (H0), 1D hole (H1) and 2D hole (H2). Red lines indicate the holes with significantly longer lifespans compared to the threshold, corrected for multiple comparisons.

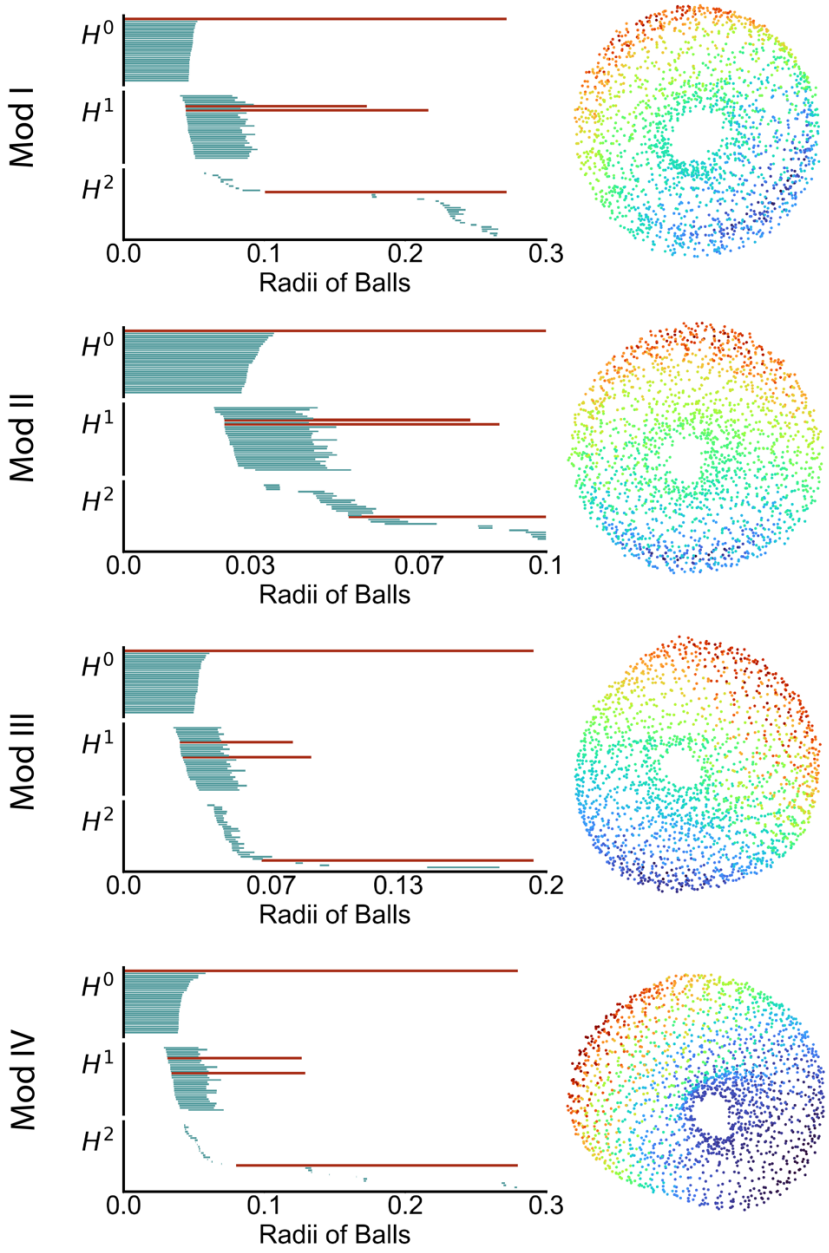

Figure S4. Illustration of the formation of hexagonal patterns during CAN simulation. a) an exemplar recurrent weight matrix that corresponds to a given location (grid Mod I). The weight was simulated by the representational oscillatory interference of elementary neuron VCOs that proposed by the oscillatory interference model. Each VCO showed a band-like or stripe-like firing patterns with preferred displacement direction over the representational space. b) schematic of the developmental procedure of hexagonal pattern during CAN model iterations. T denotes the number of spatial movements.

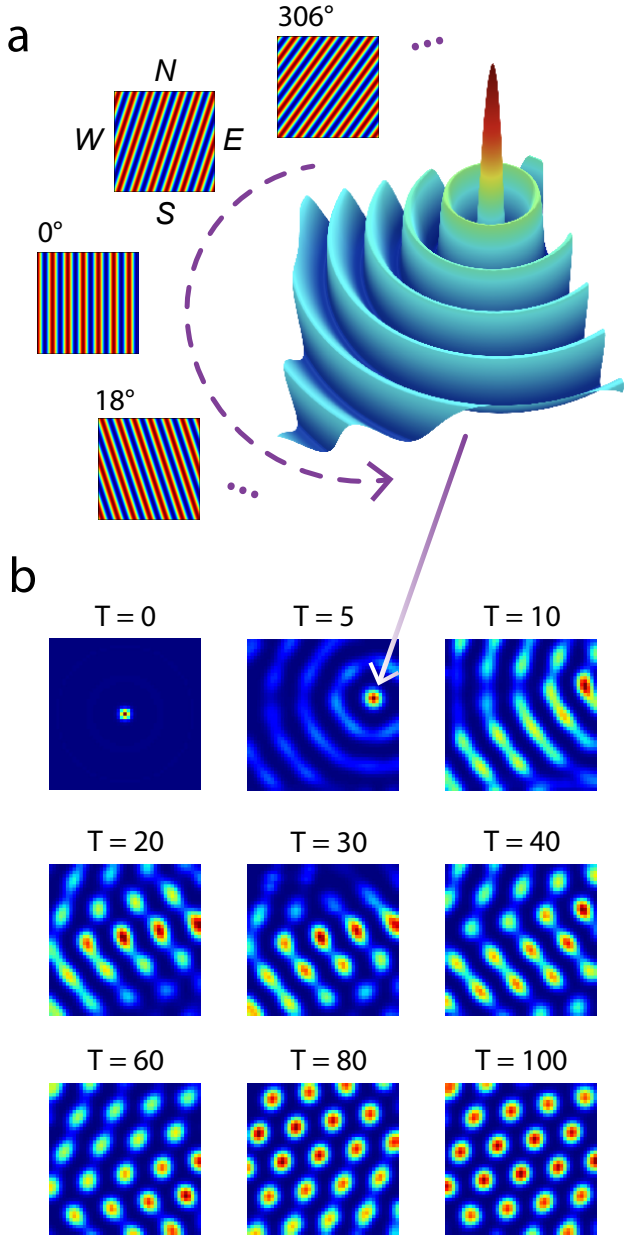

Figure S5. Simulation of periodic boundary condition. a) an exemplar hexagonal pattern used for illustration, b) Grid orientation computed from autocorrelation map of original hexagonal pattern, c) Each pixel in the blank area (highlighted in white), appeared after the phase displacement of hexagonal pattern towards the North, was interpolated with the grid activity from one out of six adjacent locations using Trigonometry, based on the grid orientation and spatial phase of the given hexagonal pattern. d) The hexagonal pattern obtained through interpolation with its spatial phase shifted towards the North.

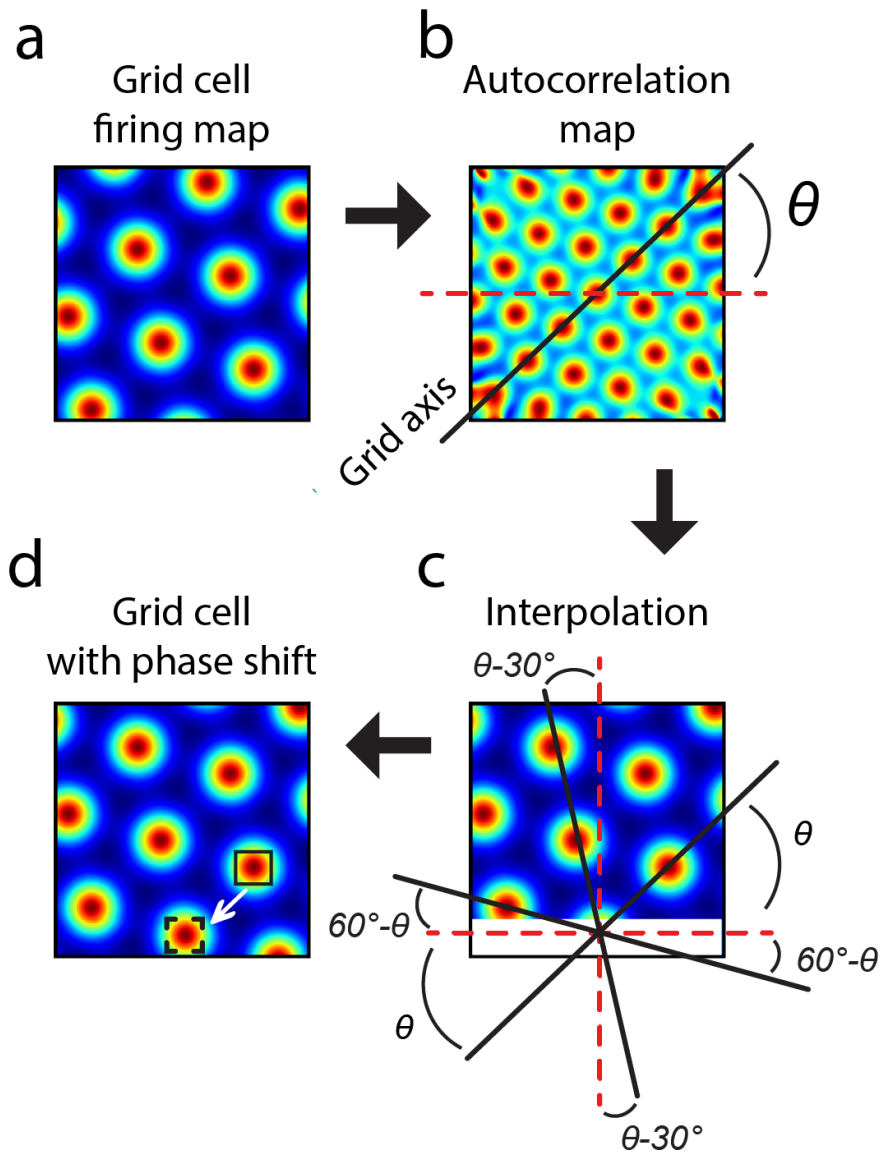

Figure S6. Effect of the amount of experience and grid scale on hexagonal regularity. Grid scales were quantified by the number of pixels. Black/Red lines represent the models with No-/Reverse-replay applied, respectively. Dashed line indicates the significance threshold of grid score. Error bar denotes the standard error of 12 independent simulations.

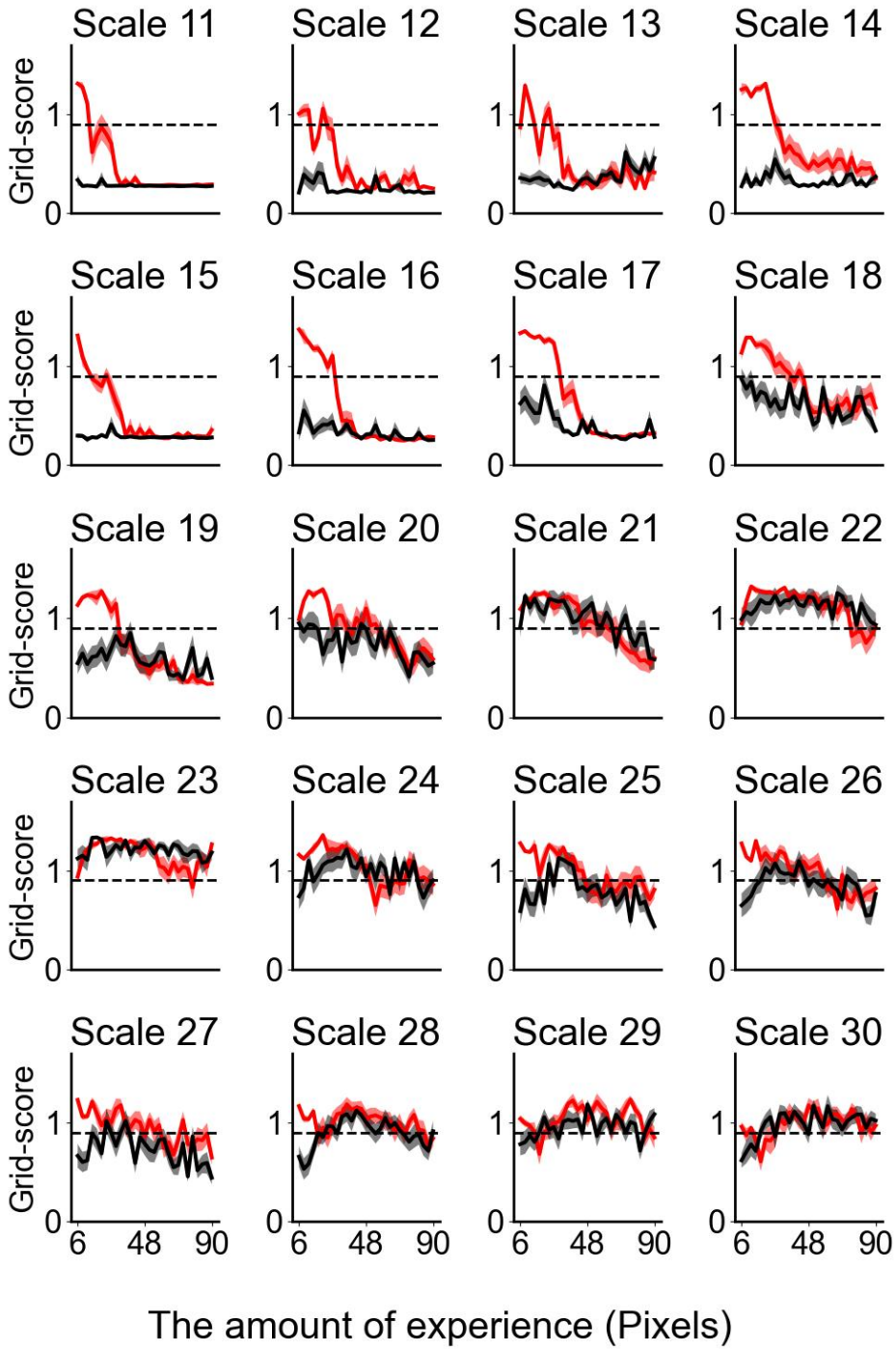

Figure S7. Grid scores changed as a function of grid scales and iterations. Grid scales were quantified by the number of pixels. Large-scale hexagonal regularity increases faster than that of small-scales. Red line indicates the iteration where grid score reached the significance threshold. Error bar denotes the standard error of 12 independent simulations.

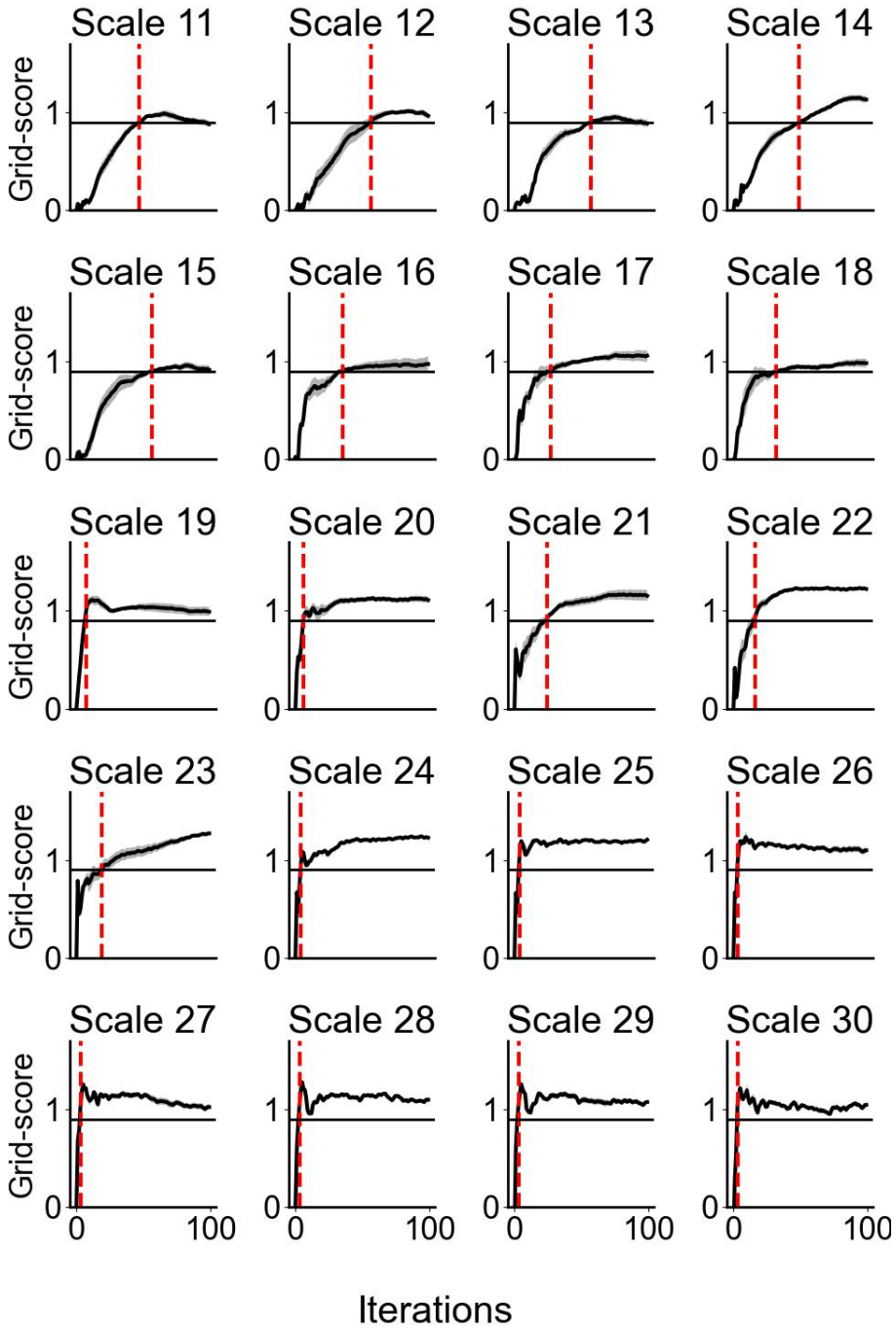

Figure S8. Movement trajectories used for hexagonal pattern simulation in each of No-replay and Reverse-replay. The trajectories were generated by a series of “walking” experiences with each defined by a unique global direction plus a noise ranged from -90° to 90°. Left column: directional distribution of each trajectory, black solid line indicates the mean of directions. Right column: the actual trajectories projected on a squared space.

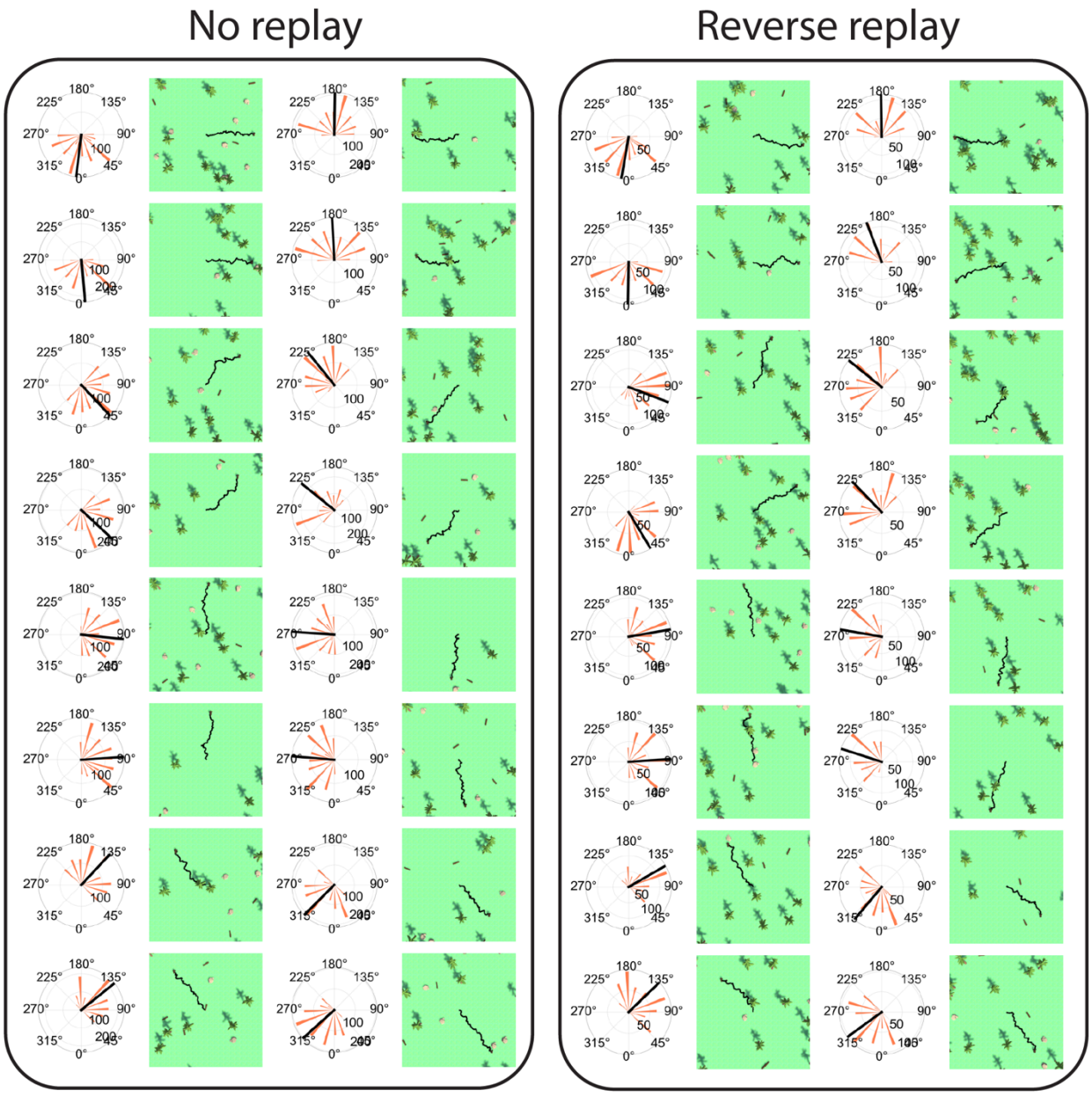

Figure S9. Procedure of field-shuffling permutation. 1) an example of hexagonal pattern, 2) extracting the peaks of the firing field, 3) identifying the local structure of hexagonal pattern, outlined by polygons using Voronoi polygons, 4-5) the firing field that was randomly re-positioned during field-shuffling, (6) the shuffled hexagonal pattern of grid cell, (7) the grid score distribution derived from 100 field-shuffling, the black dash line represents the initial (uncorrected) threshold at the 99th percentile of grid score distribution, (8) the uncorrected grid score distribution derived from grid cell population, black dash line represents the corrected threshold for multiple comparisons at the 95th percentile of the distribution.

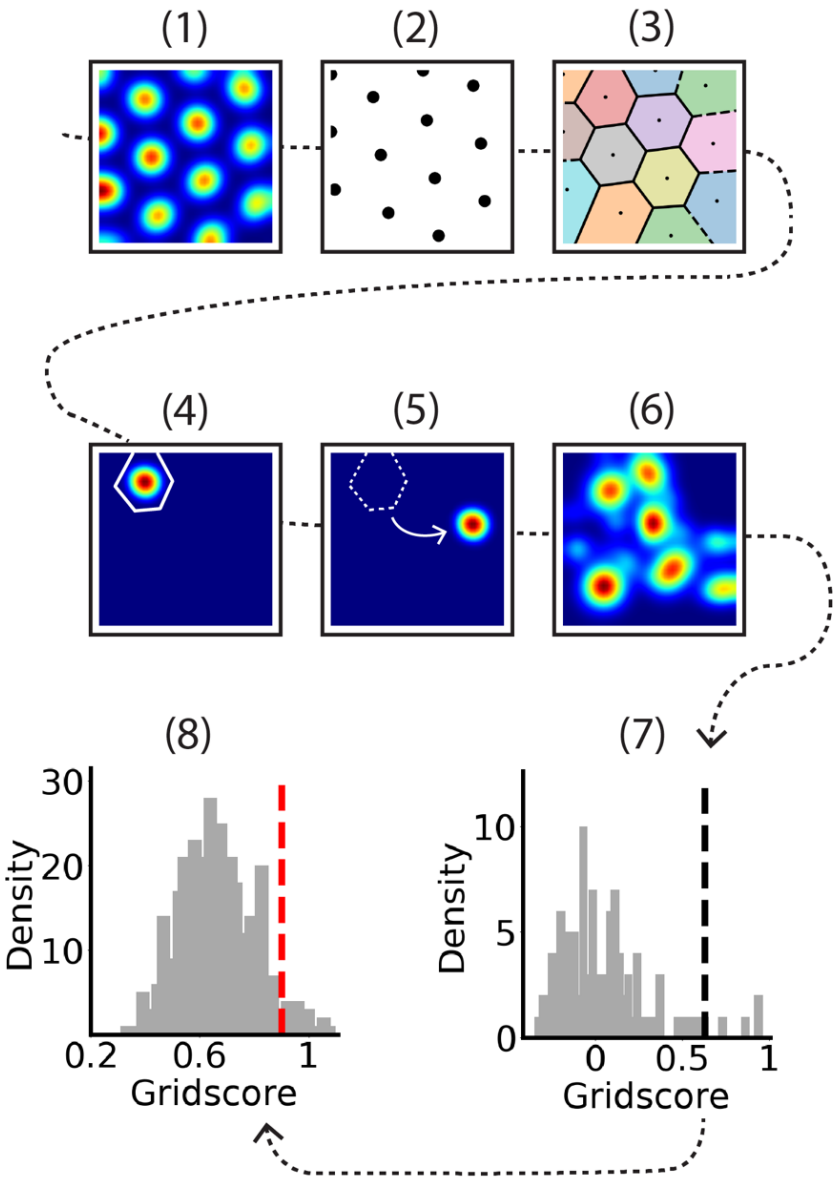

Table S1. Model parameters.

Parameter	Variable	Value
Membrane voltage threshold	η	0
Time constant	τ	10
Weight matrix	W	
Positive peak		0.003
Negative peak		-0.001
Mean		0
Amplitude of planar wave	α	0.333
Grid scales	$\vec{\sigma}$	11-30 pixels (20 samples)
Space size	N	45 pixels